Supporting Information

Content

1. Synthesis of the cage compounds

According to our previously reported methods,[1] each cage compound $[BF_4@Pd_4\mathbf{L}^{1\text{-}4}{}_8](BF_4)_7$ was formed in quantitative yield by heating a mixture of the corresponding Ligand ($\mathbf{L}^1$: 1.36 mg, 1.4 µmol; $\mathbf{L}^2$: 1.40 mg, 1.4 µmol; $\mathbf{L}^3$: 1.45 mg, 1.4 µmol and $\mathbf{L}^4$: 0.57, 1.4 µmol) and a solution of $[Pd(CH_3CN)_4](BF_4)_2$ (0.68 µmol, 45 µL of a 15 mM stock solution in CD_3CN) in CD_3CN (450 µL) at 70 °C for 24 h in a closed vial to give a 0.35 mM solution of the double-cage.

2. Titration experiments

The host-guest complexes were formed by titrating a solution of the halide anions (as their tetra-*n*-butylammonium salts in CD_3CN, 17.5 mM) in steps of 1.0 eq into 500 µL of a 0.35 mM solution of the cages in CD_3CN in an NMR tube. The NMR spectra were recorded immediately after briefly shaking the solution.

Silver ion back-titrations: By addition of Ag(I) ions to the solution containing $[2X+BF_4@Pd_4\mathbf{L}^{1\text{-}4}{}_8](BF_4)_5$, either AgCl or AgBr were precipitated. For the cage based on dibenzosuberone ($\mathbf{L}^4$), 28 equiv. of Ag(I) ions were needed for the complete precipitation of AgCl from the host-guest complex with chloride,[2] whereas the chloride-containing host-guest complexes based on the phenothiazine ligands ($\mathbf{L}^{1\text{-}3}$) show a complete precipitation upon addition of 2 equiv. of Ag(I). For the precipitation of AgBr from the bromide-containing host-guest complexes, only two equiv. of Ag(I) were needed for all examined double-cages.

A. $[BF_4@Pd_4L^1{}_8](BF_4)_7$

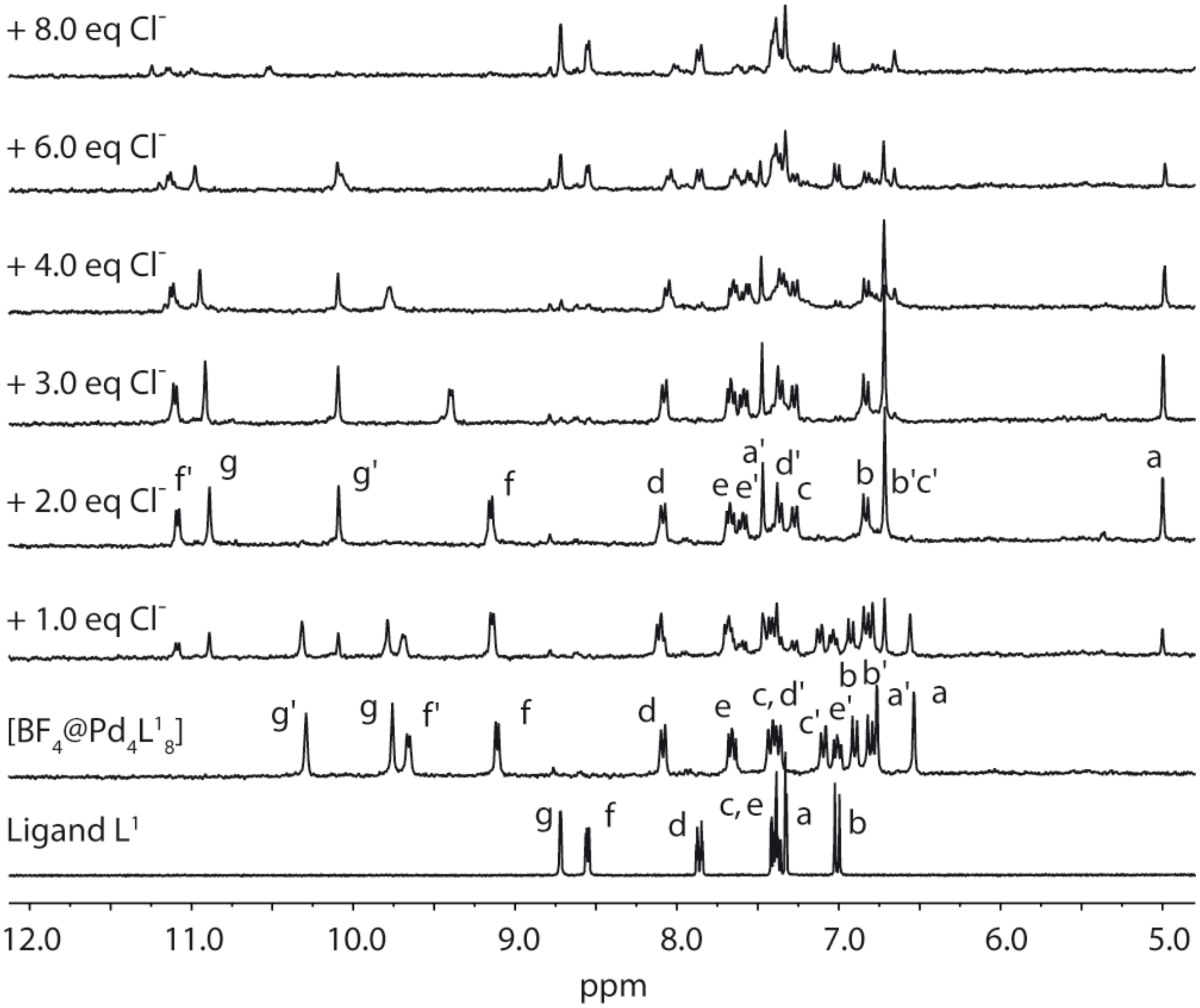

Figure SI-1: ^1H NMR titration (300 MHz, 298 K, CD_3CN) of $[BF_4@Pd_4\mathbf{L^1}_8](BF_4)_7$ with NBu_4Cl (17.5 mM). Upon addition of two equivalents of Cl^-, $[BF_4@Pd_4\mathbf{L^1}_8](BF_4)_7$ transforms into $[2Cl{+}BF_4@Pd_4\mathbf{L^1}_8](BF_4)_5$. Further addition of excess halide results in decomplexation of Pd(II) under release of free ligand **1**.

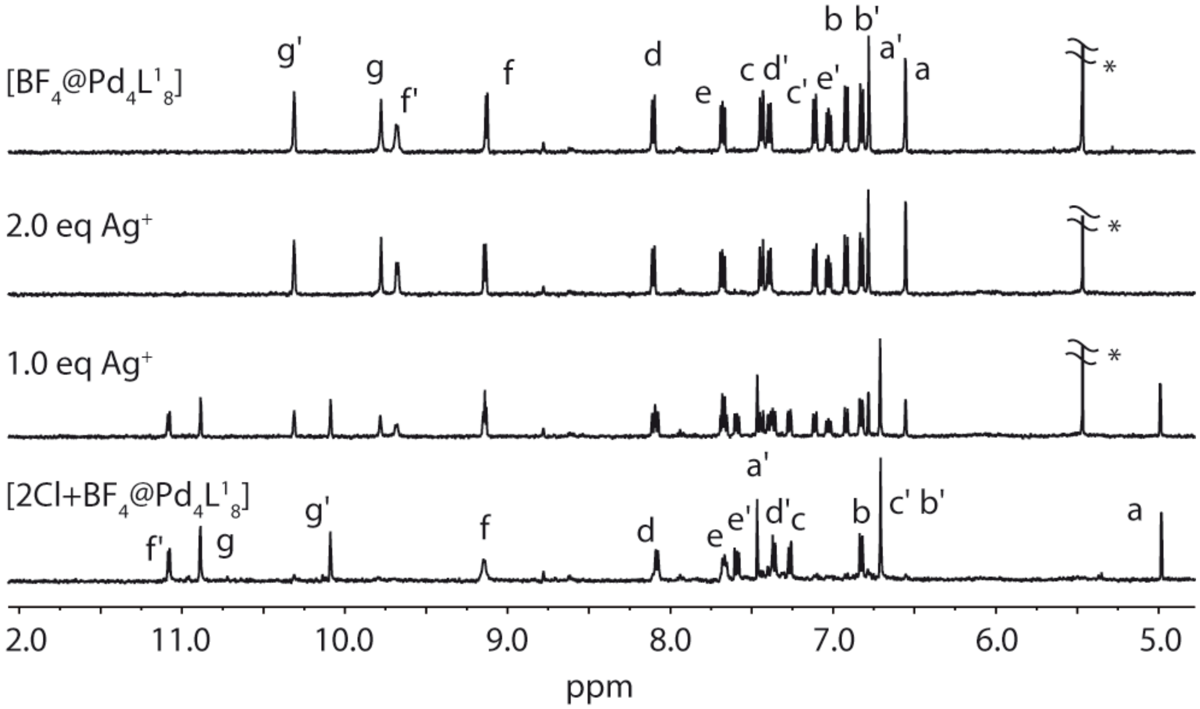

Figure SI-2: ^{1}H NMR titration (500 MHz, 298 K, CD_3CN): Precipitation of encapsulated chloride from $[2Cl+BF_4@Pd_4\mathbf{L^1}_8](BF_4)_5$ with two equivalents of $AgBF_4$ under full recovery of $[BF_4@Pd_4\mathbf{L^1}_8](BF_4)_7$ (top spectrum as reference).

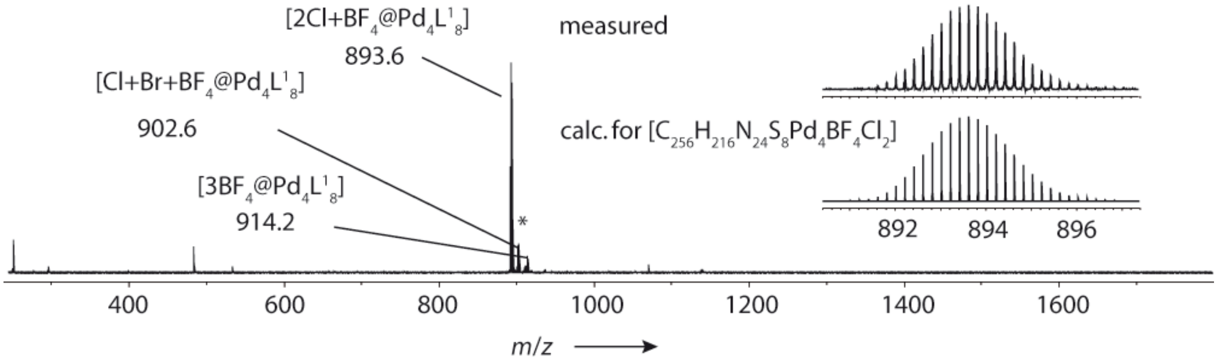

Figure SI-3: ESI mass spectrum (FTICR, positive mode, eluent CH_3CN) of the host-guest-complex $[2Cl+BF_4@Pd_4\mathbf{L^1}_8](BF_4)_5$. * = contamination with Br^-.

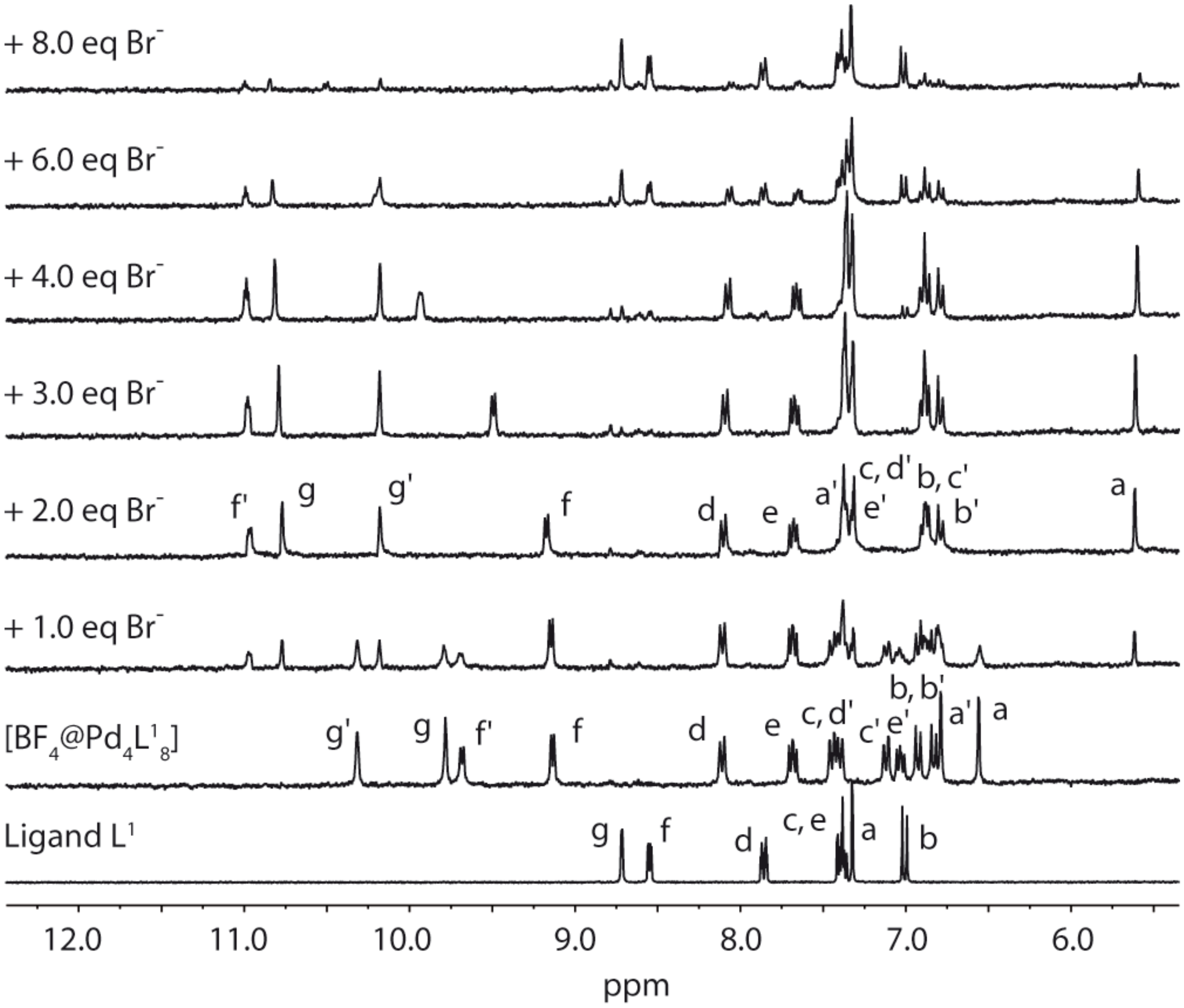

Figure SI-4: ^{1}H NMR titration (300 MHz, 298 K, CD_3CN) of $[BF_4@Pd_4\mathbf{L^1}_8](BF_4)_7$ with NBu_4Br (17.5 mM). Upon addition of two equivalents of Br^-, $[BF_4@Pd_4\mathbf{L^1}_8](BF_4)_7$ transforms into $[2Br+BF_4@Pd_4\mathbf{L^1}_8](BF_4)_5$. Further addition of excess halide results in decomplexation of Pd(II) under release of free ligand $\mathbf{L^1}$.

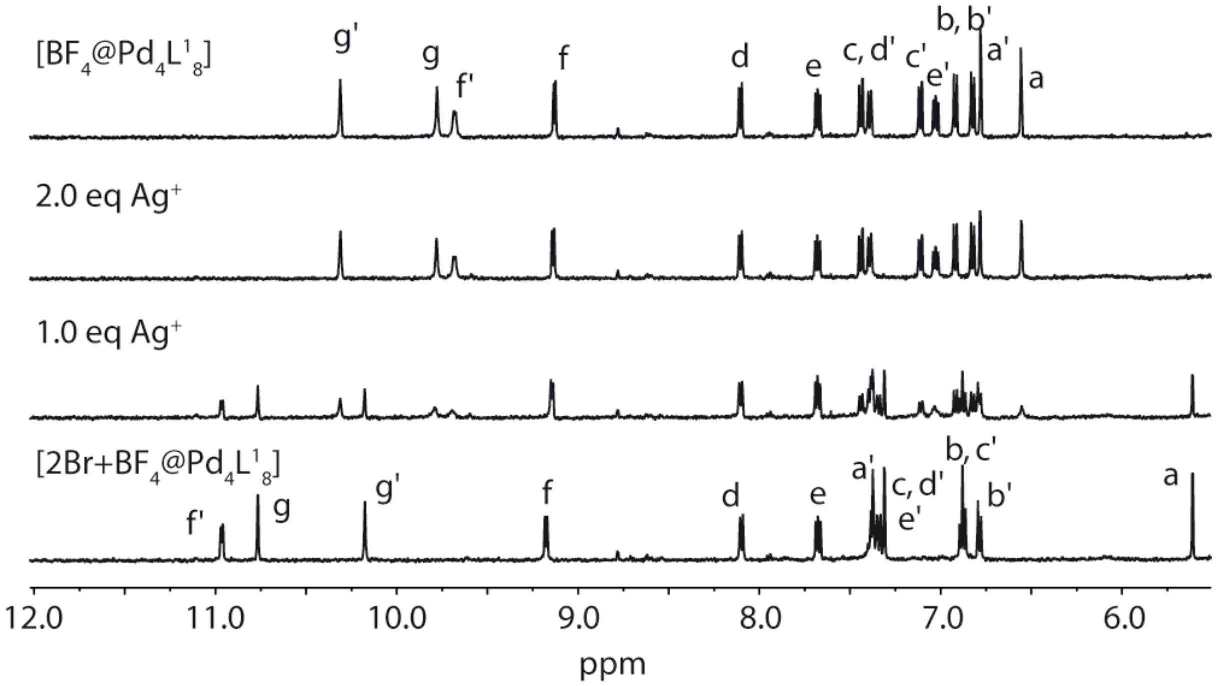

Figure SI-5: ^{1}H NMR titration (500 MHz, 298 K, CD_3CN): Precipitation of encapsulated chloride from [2Br+BF_4@$Pd_4$$\mathbf{L}^{\mathbf{1}}_8$]$(BF_4)_5$ with two equivalents of $AgBF_4$ under full recovery of [BF_4@$Pd_4$$\mathbf{L}^{\mathbf{1}}_8$]$(BF_4)_7$ (top spectrum as reference).

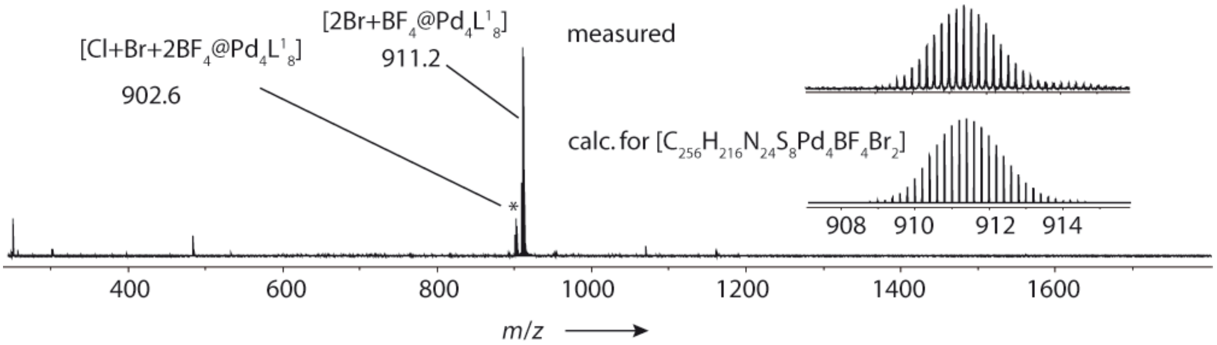

Figure SI-6: ESI mass spectrum (FTICR, positive mode, eluent CH_3CN) of the host-guest-complex [2Br+BF_4@$Pd_4$$\mathbf{L}^{\mathbf{1}}_8$]$(BF_4)_5$. * = contamination with Cl^-.

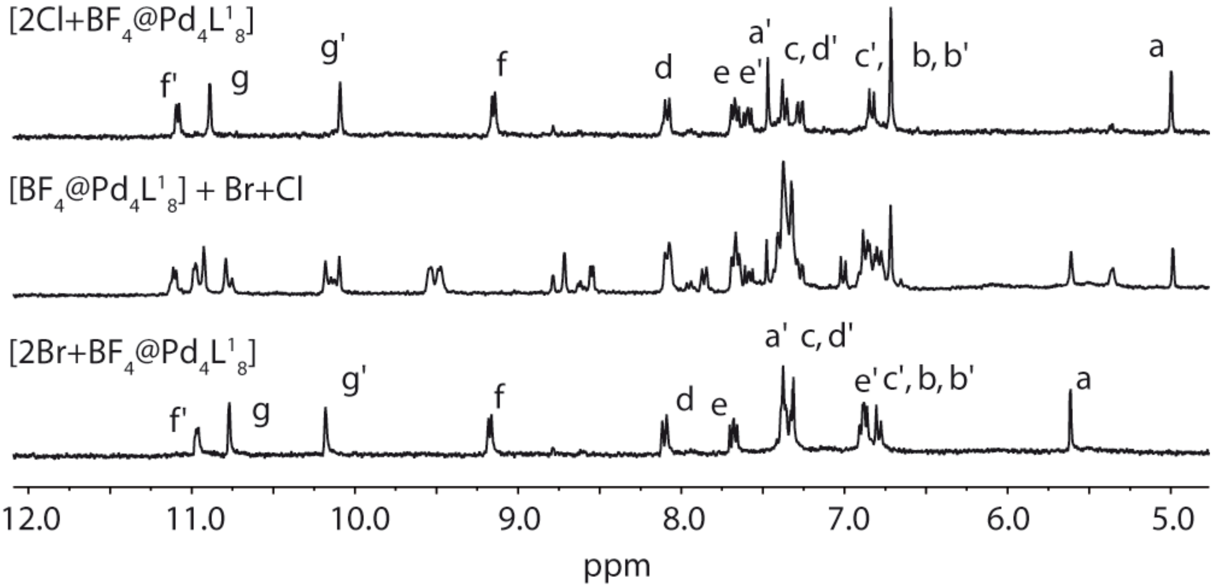

Figure SI-7: ^{1}H NMR titration (300 MHz, 298 K, CD_3CN): Competition of two equivalents of bromide with chloride for the binding by $[BF_4@Pd_4\mathbf{L^1}_8](BF_4)_7$. Signals of $[2Br+BF_4@Pd_4\mathbf{L^1}_8](BF_4)_5$ and $[2Cl+BF_4@Pd_4\mathbf{L^1}_8](BF_4)_5$ show almost the same intensity, indicating that a comparable affinity of $[BF_4@Pd_4\mathbf{L^1}_8](BF_4)_7$ for both halide anions. Signals of free Ligand $\mathbf{L^1}$ also start to appear.

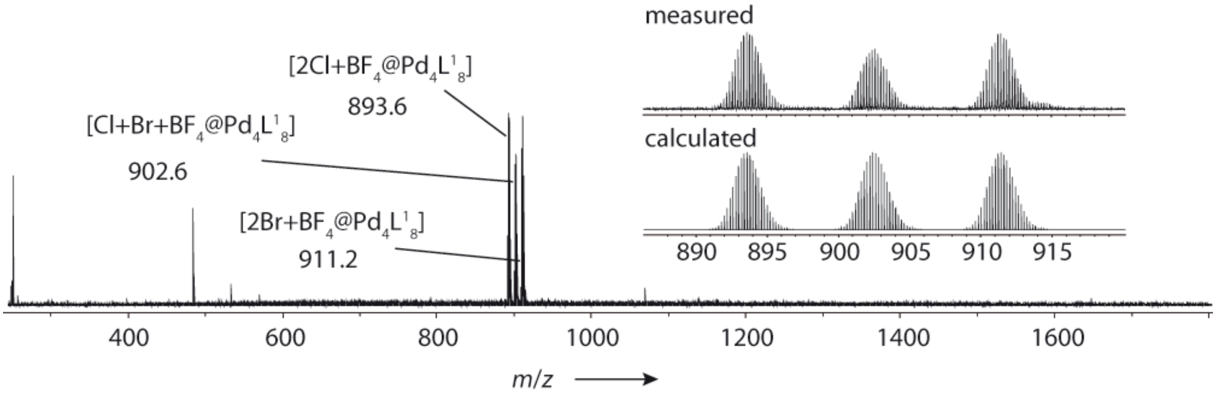

Figure SI-8: ESI mass spectrum (FTICR, positive mode, eluent CH_3CN) of the chloride and bromide containing mixture showing equally intense signals for the host-guest-complexes $[2Br+BF_4@Pd_4\mathbf{L^1}_8](BF_4)_5$, $[Br+Cl+BF_4@Pd_4\mathbf{L^1}_8](BF_4)_5$ and $[2Cl+BF_4@Pd_4\mathbf{L^1}_8](BF_4)_5$.

B. [BF$_4$@Pd$_4$L$^3_8$](BF$_4$)$_7$

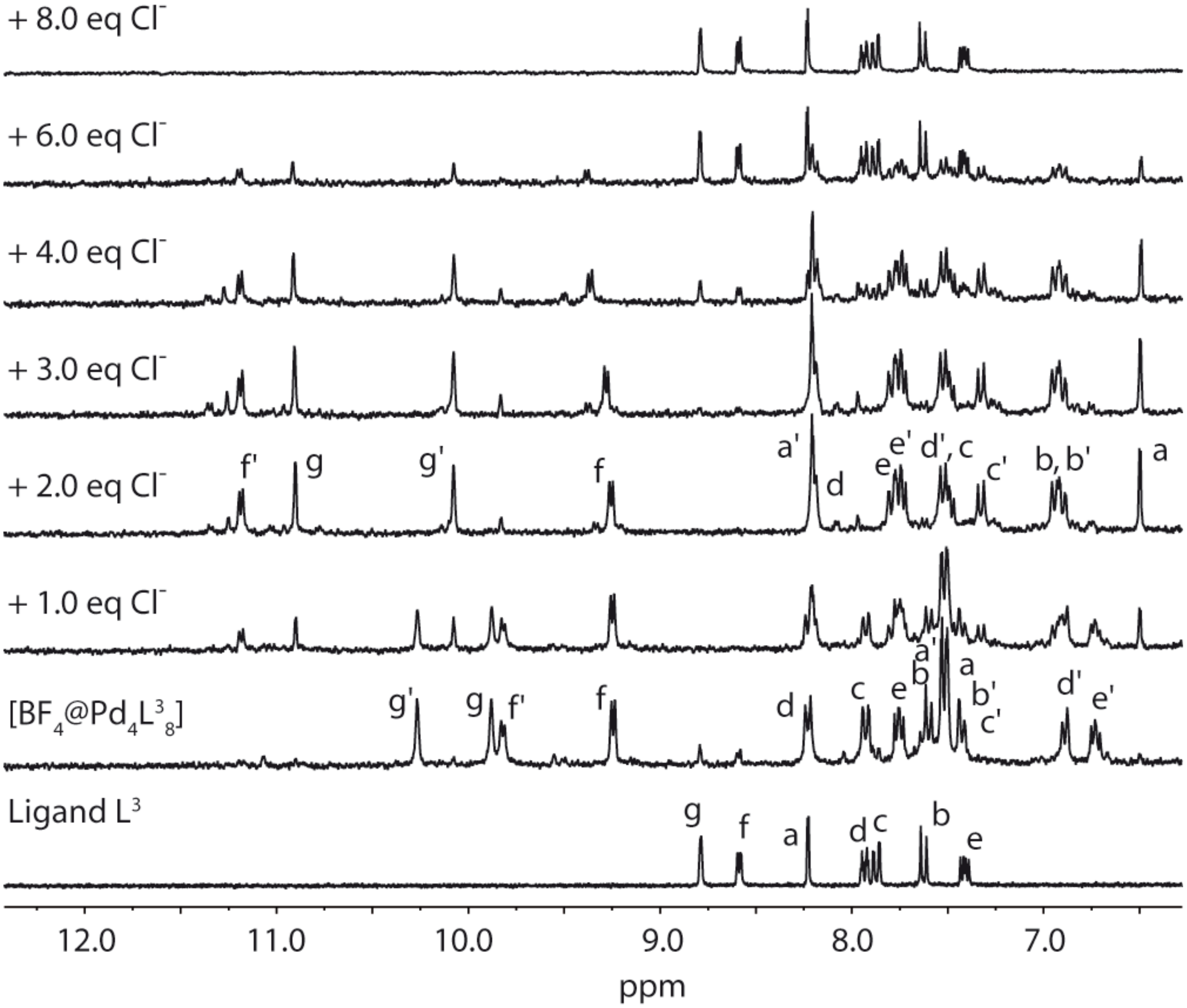

Figure SI-9: ^{1}H NMR titration (300 MHz, 298 K, CD$_3$CN) of [BF$_4$@Pd$_4$**L^3**$_8$](BF$_4$)$_7$ with NBu$_4$Cl (17.5 mM). Upon addition of two equivalents of Cl$^-$, [BF$_4$@Pd$_4$**L^3**$_8$](BF$_4$)$_7$ transforms into [2Cl+BF$_4$@Pd$_4$**L^3**$_8$](BF$_4$)$_5$. Further addition of excess halide results in decomplexation of Pd(II) under release of free ligand **L^3**.

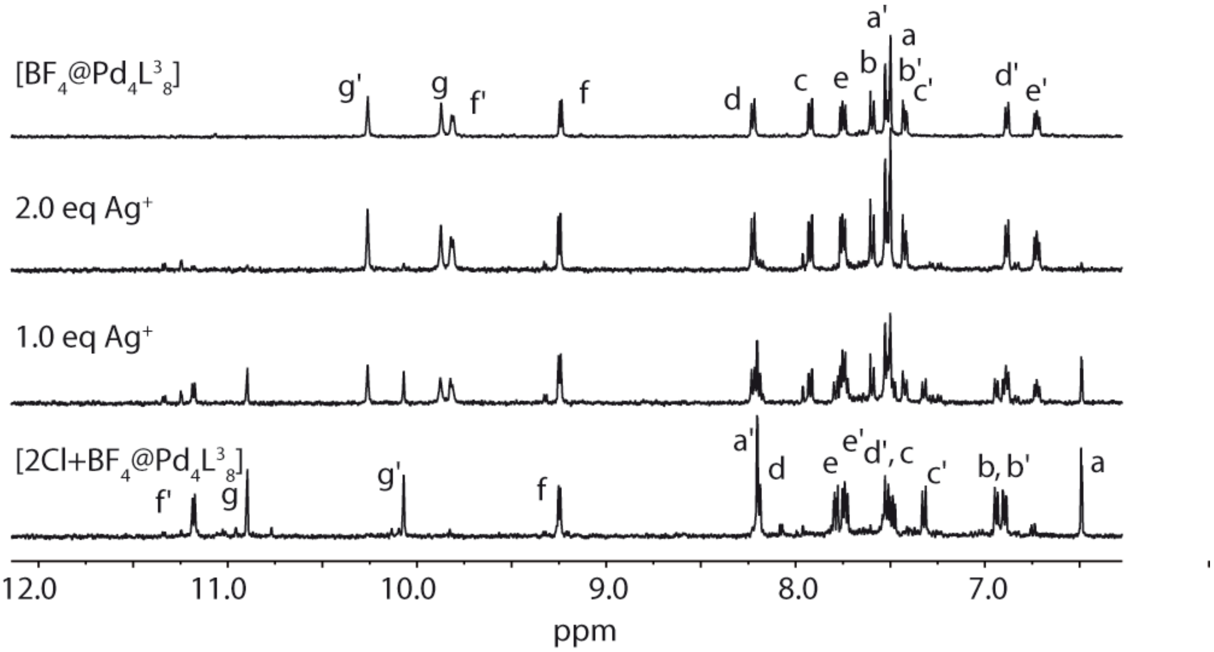

Figure SI-10: ^{1}H NMR titration (500 MHz, 298 K, CD_3CN): Precipitation of encapsulated chloride from $[2Cl+BF_4@Pd_4\mathbf{L^3}_8](BF_4)_5$ with two equivalents of $AgBF_4$ under full recovery of $[BF_4@Pd_4\mathbf{L^3}_8](BF_4)_7$ (top spectrum as reference).

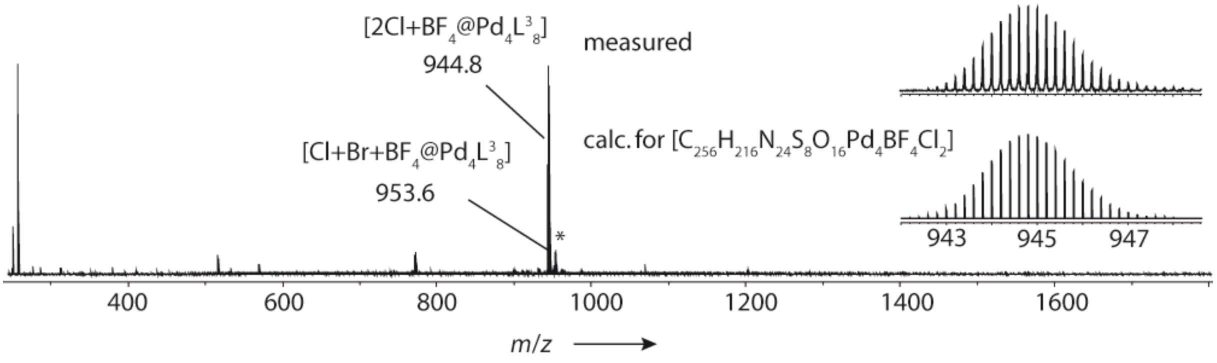

Figure SI-11: ESI mass spectrum (FTICR, positive mode, eluent CH_3CN) of the host-guest-complex $[2Cl+BF_4@Pd_4\mathbf{L^3}_8](BF_4)_5$. * = contamination with Br^-.

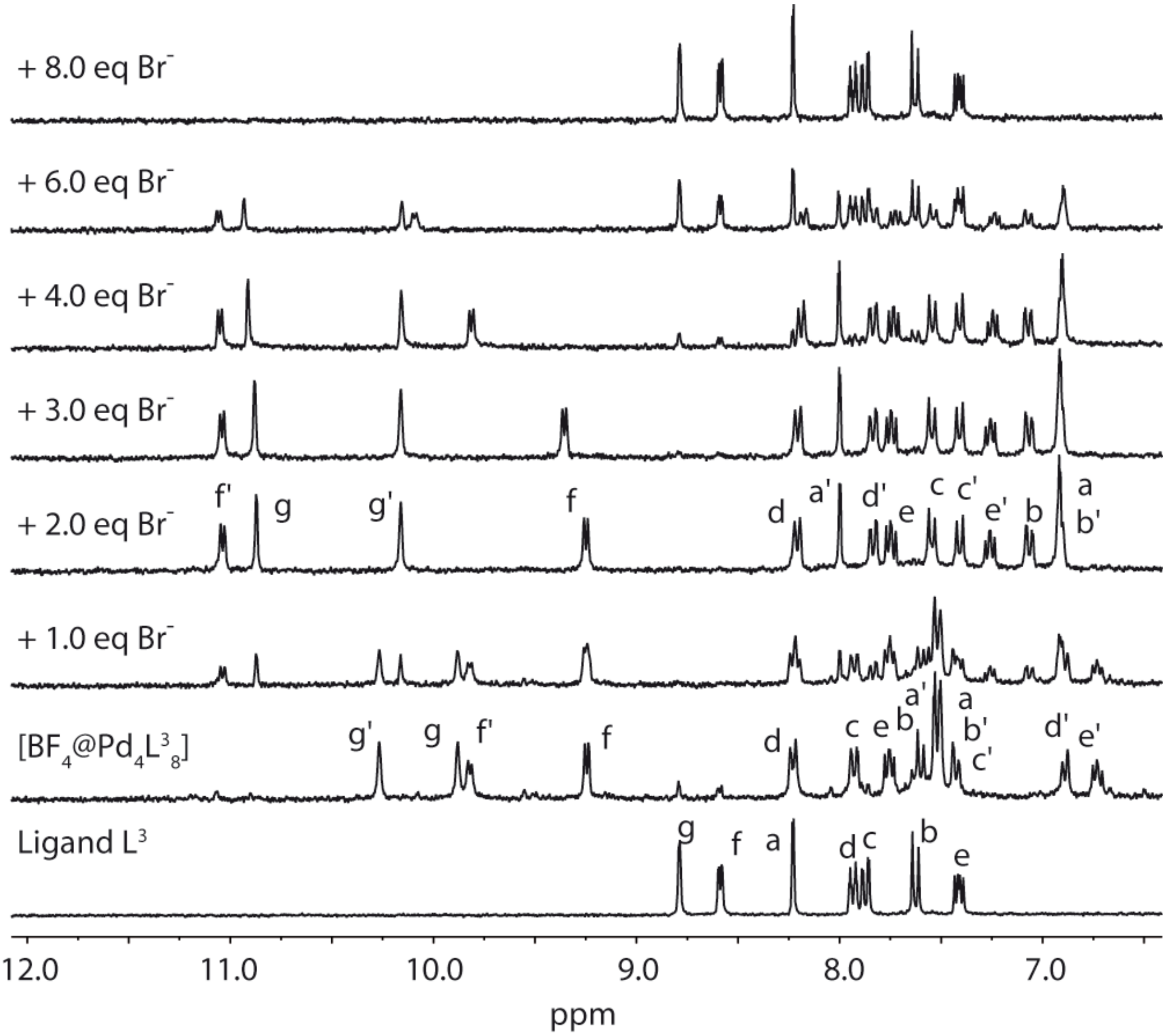

Figure SI-12: ^{1}H NMR titration (300 MHz, 298 K, CD$_3$CN) of $[BF_4@Pd_4\mathbf{L}^3_8](BF_4)_7$ with NBu$_4$Br (17.5 mM). Upon addition of two equivalents of Br$^-$, $[BF_4@Pd_4\mathbf{L}^3_8](BF_4)_7$ transforms into $[2Br+BF_4@Pd_4\mathbf{L}^3_8](BF_4)_5$. Further addition of excess halide results in decomplexation of Pd(II) under release of free ligand $\mathbf{L}^3$.

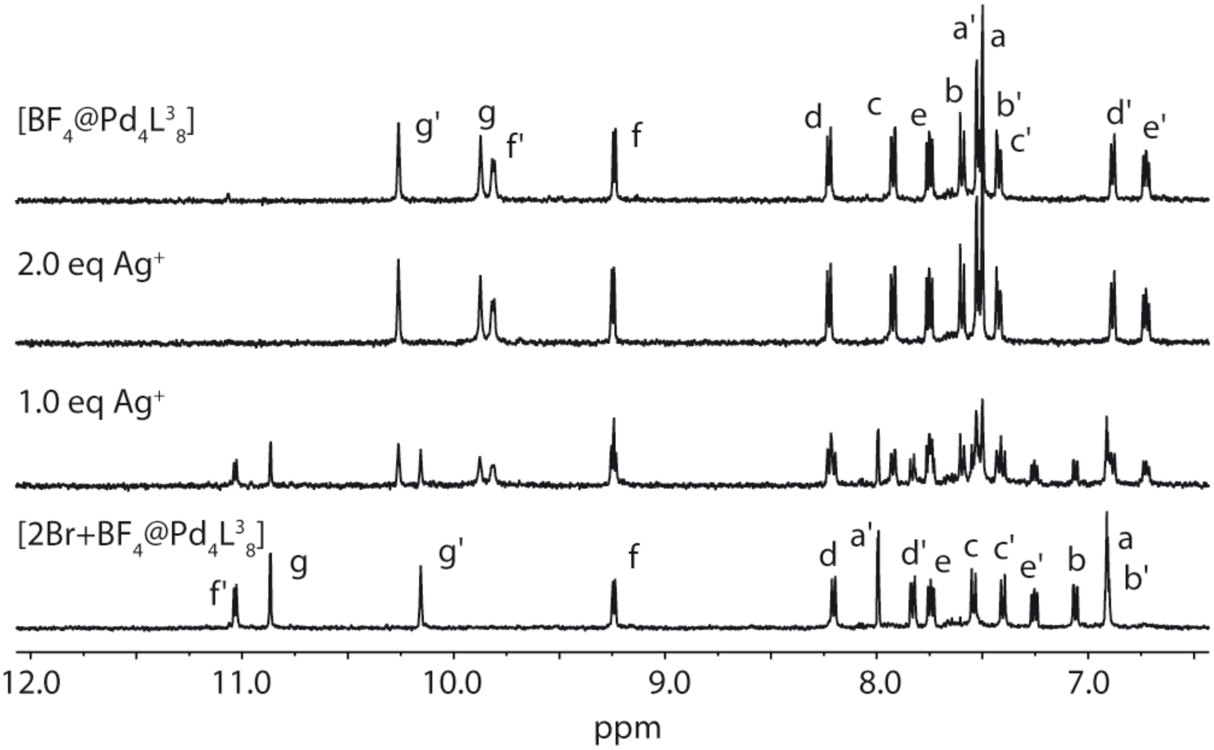

Figure SI-13: ^{1}H NMR titration (500 MHz, 298 K, CD_3CN): Precipitation of encapsulated bromide from $[2Br+BF_4@Pd_4\mathbf{L}^3_8](BF_4)_5$ with two equiv. of $AgBF_4$ under full recovery of $[BF_4@Pd_4\mathbf{L}^3_8](BF_4)_7$ (top spectrum as reference).

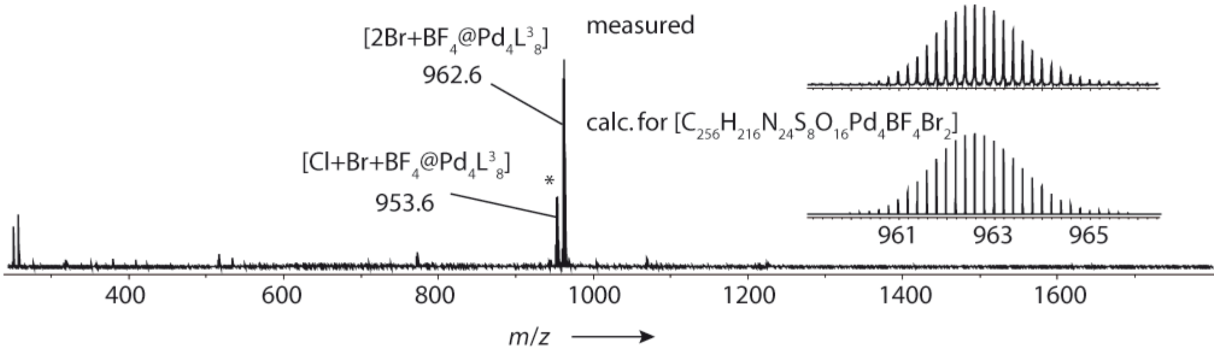

Figure SI-14: ESI mass spectrum (FTICR, positive mode, eluent CH_3CN) of the host-guest-complex $[2Br+BF_4@Pd_4\mathbf{L}^3_8](BF_4)_5$. * = contamination with Cl^-.

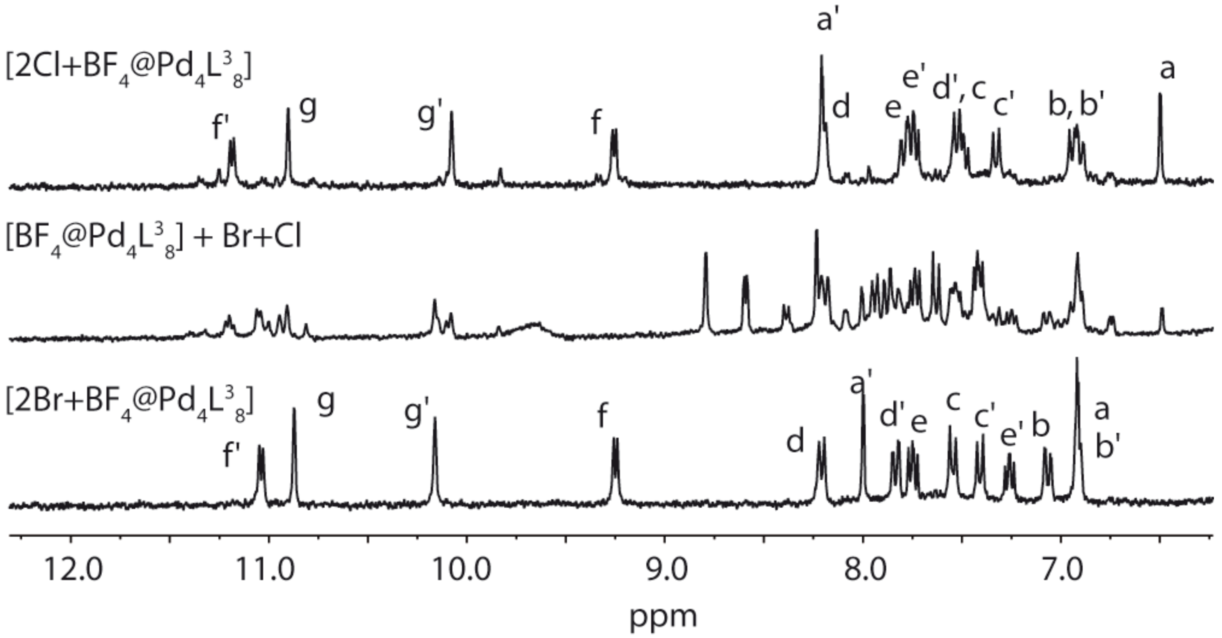

Figure SI-15: ^{1}H NMR titration (300 MHz, 298 K, CD$_3$CN): Competition of two equivalents of bromide with chloride for the binding by $[\mathrm{BF_4@Pd_4}\mathbf{L}^{3}_{8}](\mathrm{BF_4})_7$. Signals of $[\mathrm{2Br{+}BF_4@Pd_4}\mathbf{L}^{3}_{8}](\mathrm{BF_4})_5$ and $[\mathrm{2Cl{+}BF_4@Pd_4}\mathbf{L}^{3}_{8}](\mathrm{BF_4})_5$ show almost the same intensity, indicating that a comparable affinity of $[\mathrm{BF_4@Pd_4}\mathbf{L}^{3}_{8}](\mathrm{BF_4})_7$ for both halide anions. Signals of free Ligand $\mathbf{L}^{3}$ also start to appear.

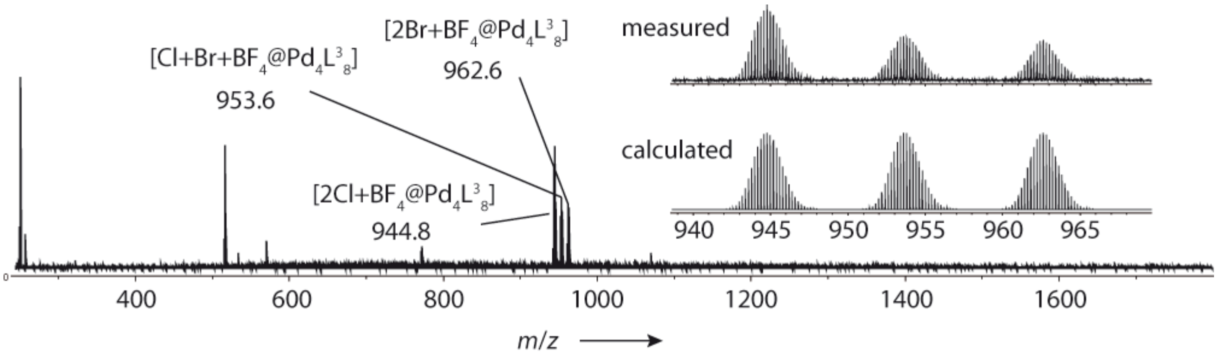

Figure SI-16: ESI mass spectrum (FTICR, positive mode, eluent CH$_3$CN) of the chloride and bromide containing mixture showing signals for the host-guest-complexes $[\mathrm{2Br{+}BF_4@Pd_4}\mathbf{L}^{3}_{8}](\mathrm{BF_4})_5$, $[\mathrm{Br{+}Cl{+}BF_4@Pd_4}\mathbf{L}^{3}_{8}](\mathrm{BF_4})_5$ and $[\mathrm{2Cl{+}BF_4@Pd_4}\mathbf{L}^{3}_{8}](\mathrm{BF_4})_5$. The latter species gives the strongest signal, indicating a preference for chloride binding in this case.

3. Cage Competition experiments

General procedure

A mixture of two different double-cages (250 µL, 0.35 mM in CD_3CN per double-cage) in a ratio of 1:1 was used for the competition experiments. This solution was treated with one equivalent of halide (with respect to the whole amount of all contained double-cages, NBu_4Cl or NBu_4Br, 17.5 mM, 10 µL in CD_3CN). The results of the individual competition experiments are printed in the top of the figures.

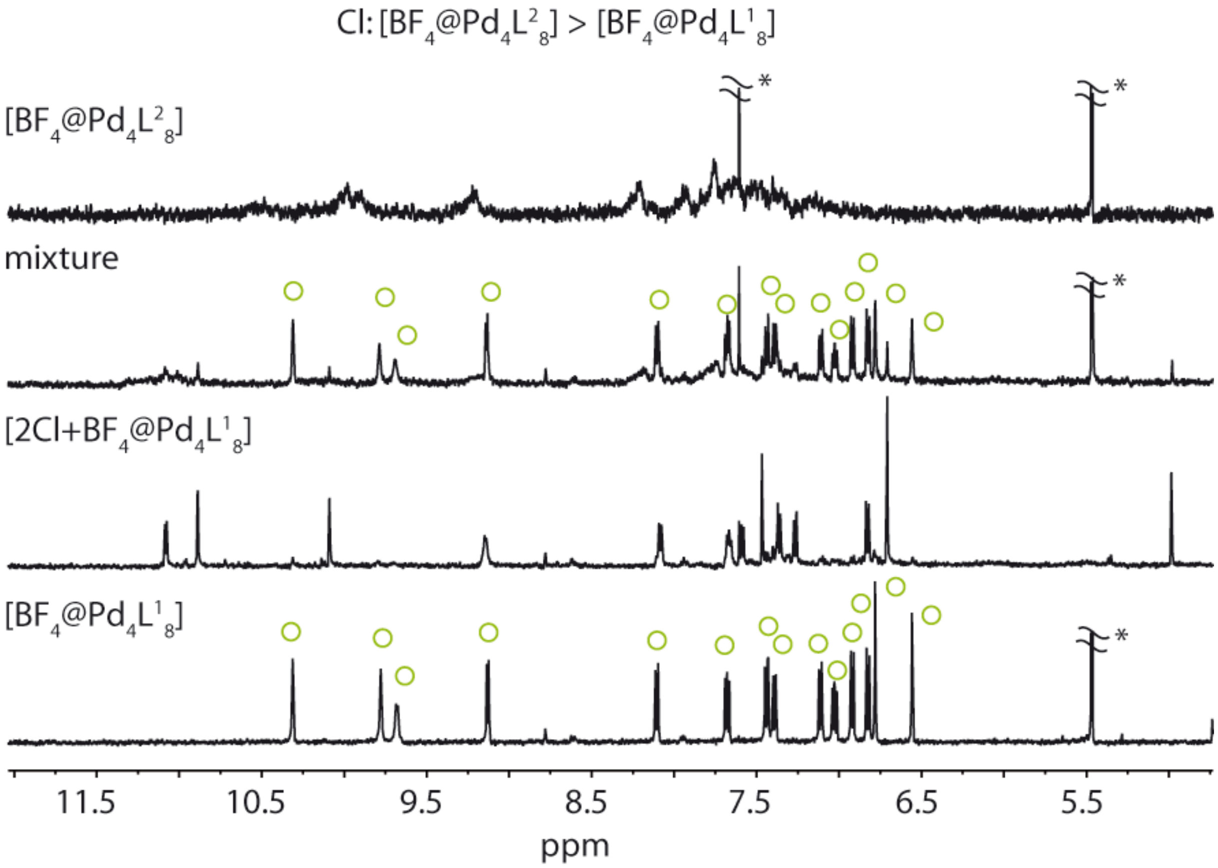

Figure SI-17: ^1H NMR titration (500 MHz, 298 K, CD_3CN): A competition experiment between $[BF_4@Pd_4\mathbf{L^1}_8](BF_4)_7$ and $[BF_4@Pd_4\mathbf{L^2}_8](BF_4)_7$ for the binding of the chloride anion shows that the latter one is the better binder. The $[BF_4@Pd_4\mathbf{L^1}_8](BF_4)_7$, $[2Cl+BF_4@Pd_4\mathbf{L^1}_8](BF_4)_5$ and $[BF_4@Pd_4\mathbf{L^2}_8](BF_4)_7$ spectra are printed as reference.

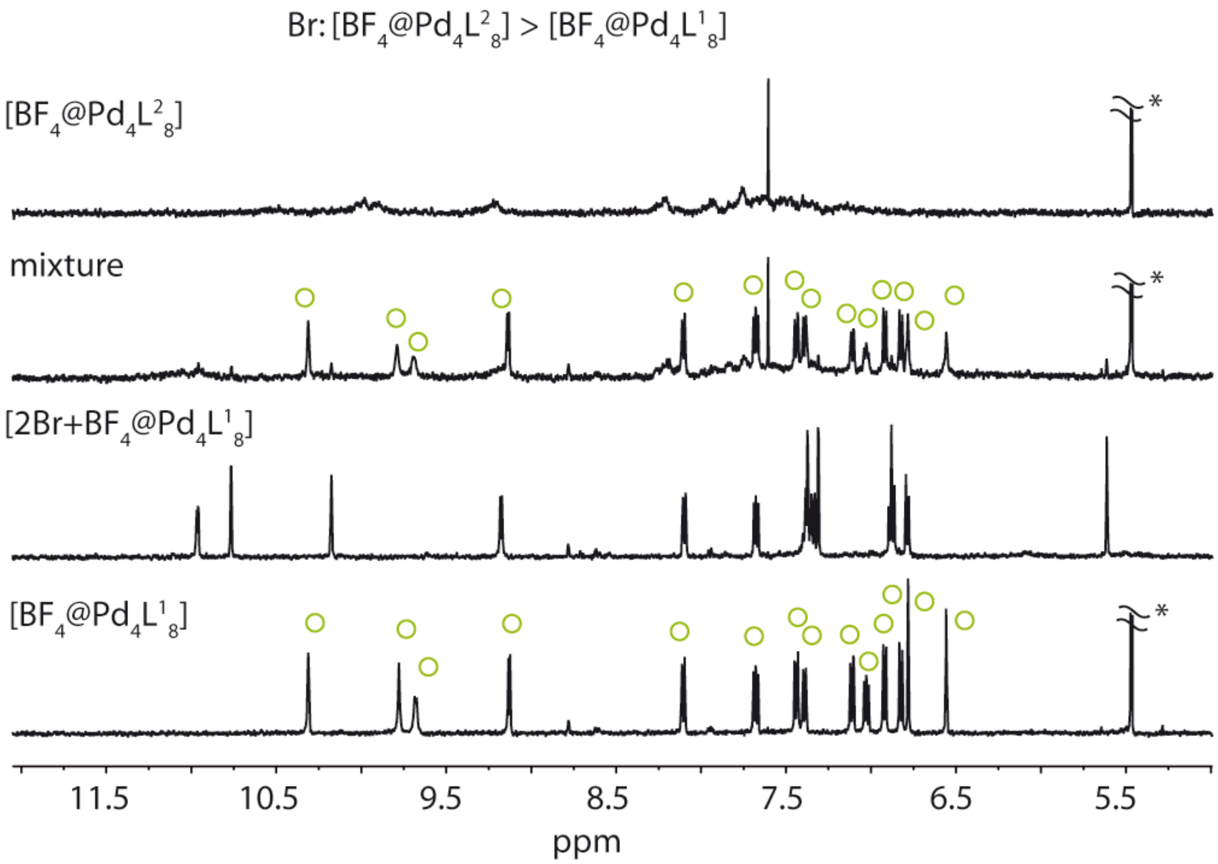

Figure SI-18: ^{1}H NMR titration (500 MHz, 298 K, CD$_3$CN): A competition experiment between [BF$_4$@Pd$_4$**L^1**$_8$](BF$_4$)$_7$ and [BF$_4$@Pd$_4$**L^2**$_8$](BF$_4$)$_7$ for the binding of the bromide anion shows that the latter one is the better binder. The [BF$_4$@Pd$_4$**L^1**$_8$](BF$_4$)$_7$, [2Br+BF$_4$@Pd$_4$**L^1**$_8$](BF$_4$)$_5$ and [BF$_4$@Pd$_4$**L^2**$_8$](BF$_4$)$_7$ spectra are printed as reference.

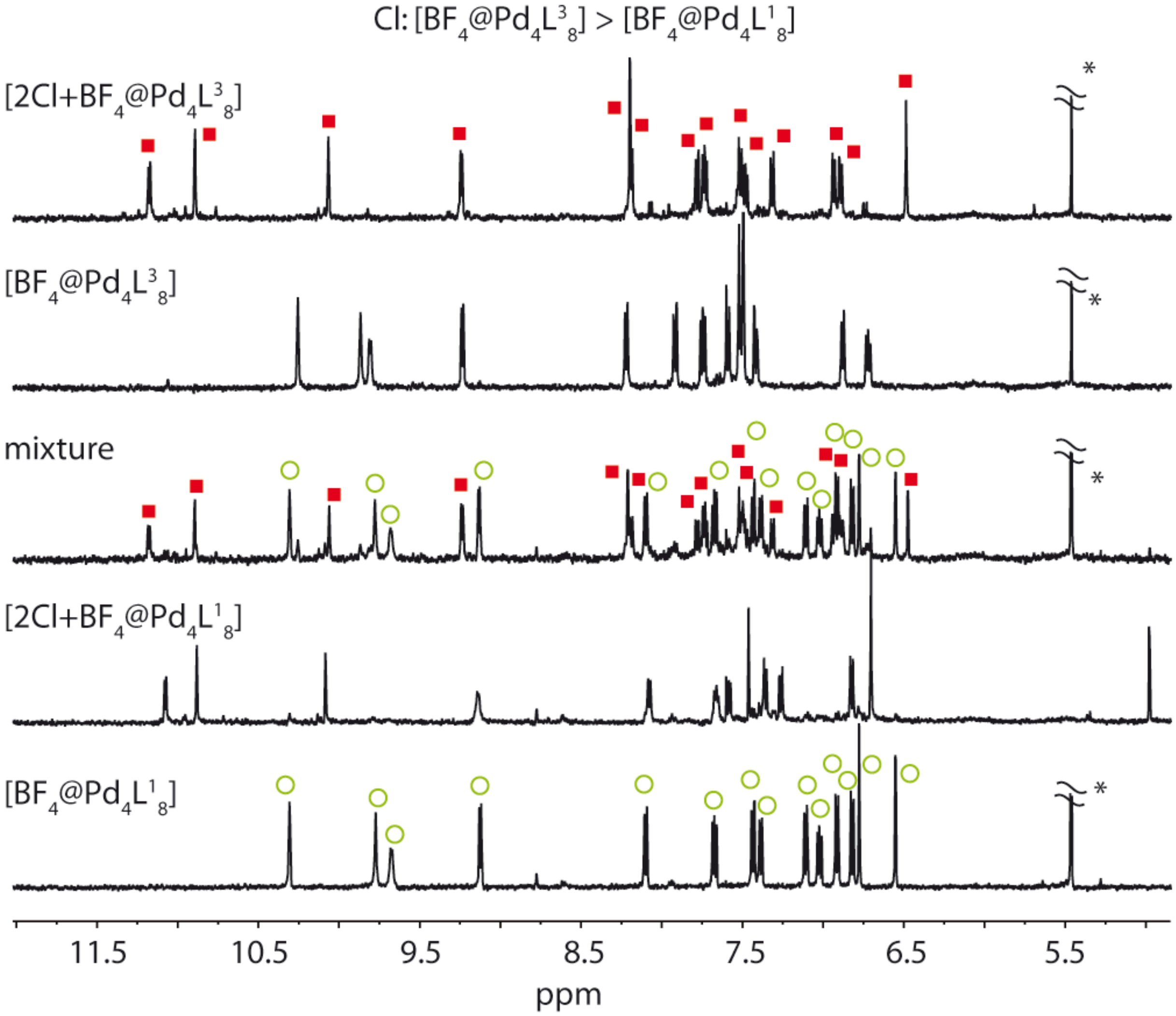

Figure SI-19: ^{1}H NMR titration (500 MHz, 298 K, CD_3CN): A competition experiment between $[BF_4@Pd_4\mathbf{L}^{\mathbf{1}}_8](BF_4)_7$ and $[BF_4@Pd_4\mathbf{L}^{\mathbf{3}}_8](BF_4)_7$ for the binding of the chloride anion shows that the latter one is the better binder. The $[BF_4@Pd_4\mathbf{L}^{\mathbf{1}}_8](BF_4)_7$, $[2Cl{+}BF_4@Pd_4\mathbf{L}^{\mathbf{1}}_8](BF_4)_5$, $[BF_4@Pd_4\mathbf{L}^{\mathbf{3}}_8](BF_4)_7$ and $[2Cl{+}BF_4@Pd_4\mathbf{L}^{\mathbf{3}}_8](BF_4)_5$ spectra are printed as reference. * = impurity.

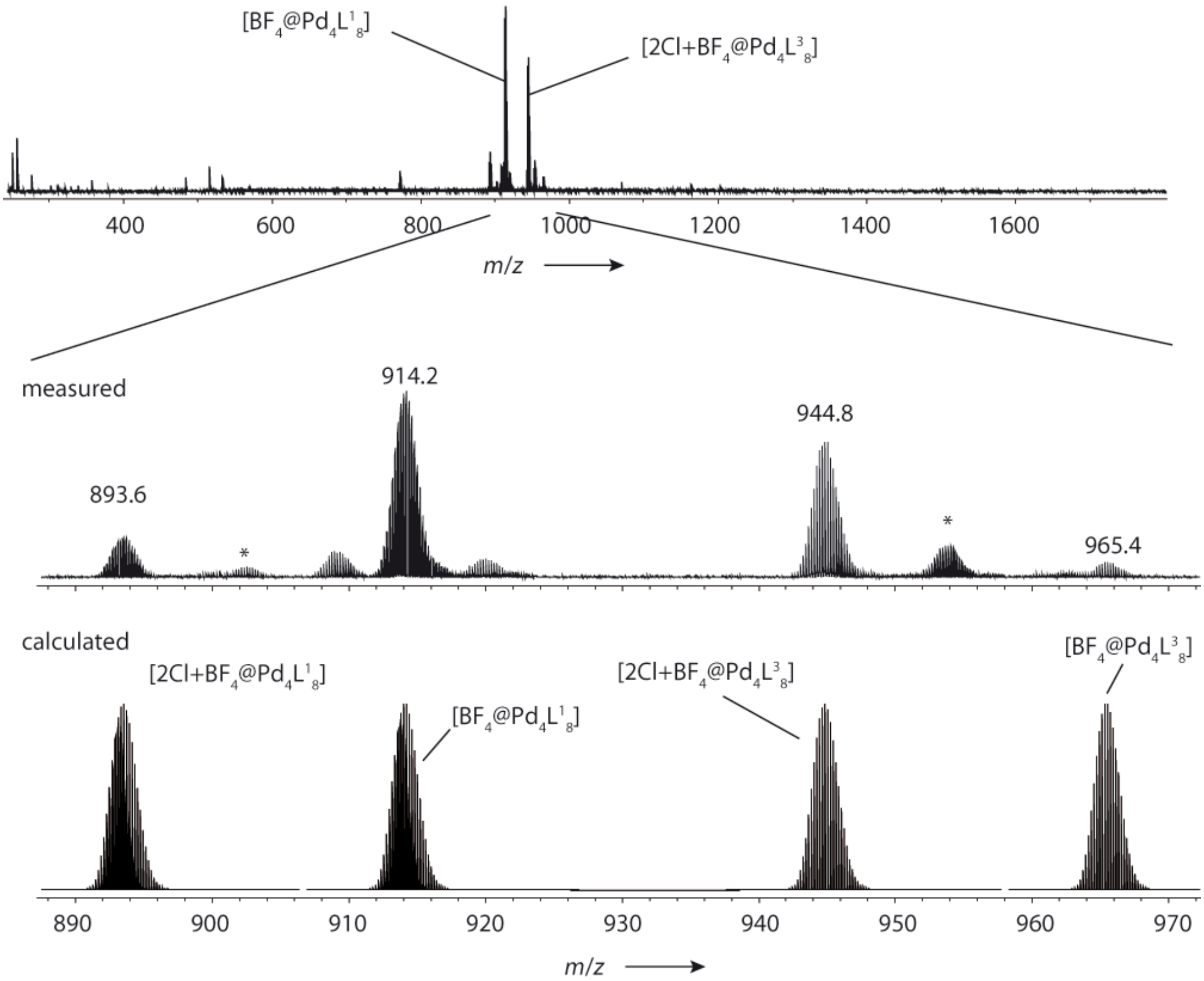

Figure SI-20: The ESI mass spectrum (FTICR, positive mode, eluent CH_3CN) of the host-guest-complexes in the competition experiment of $[BF_4@Pd_4\mathbf{L^1}_8](BF_4)_7$ and $[BF_4@Pd_4\mathbf{L^3}_8](BF_4)_7$ with NBu_4Cl clearly shows the higher affinity of the latter cage for chloride binding. * = contamination with Br^-.

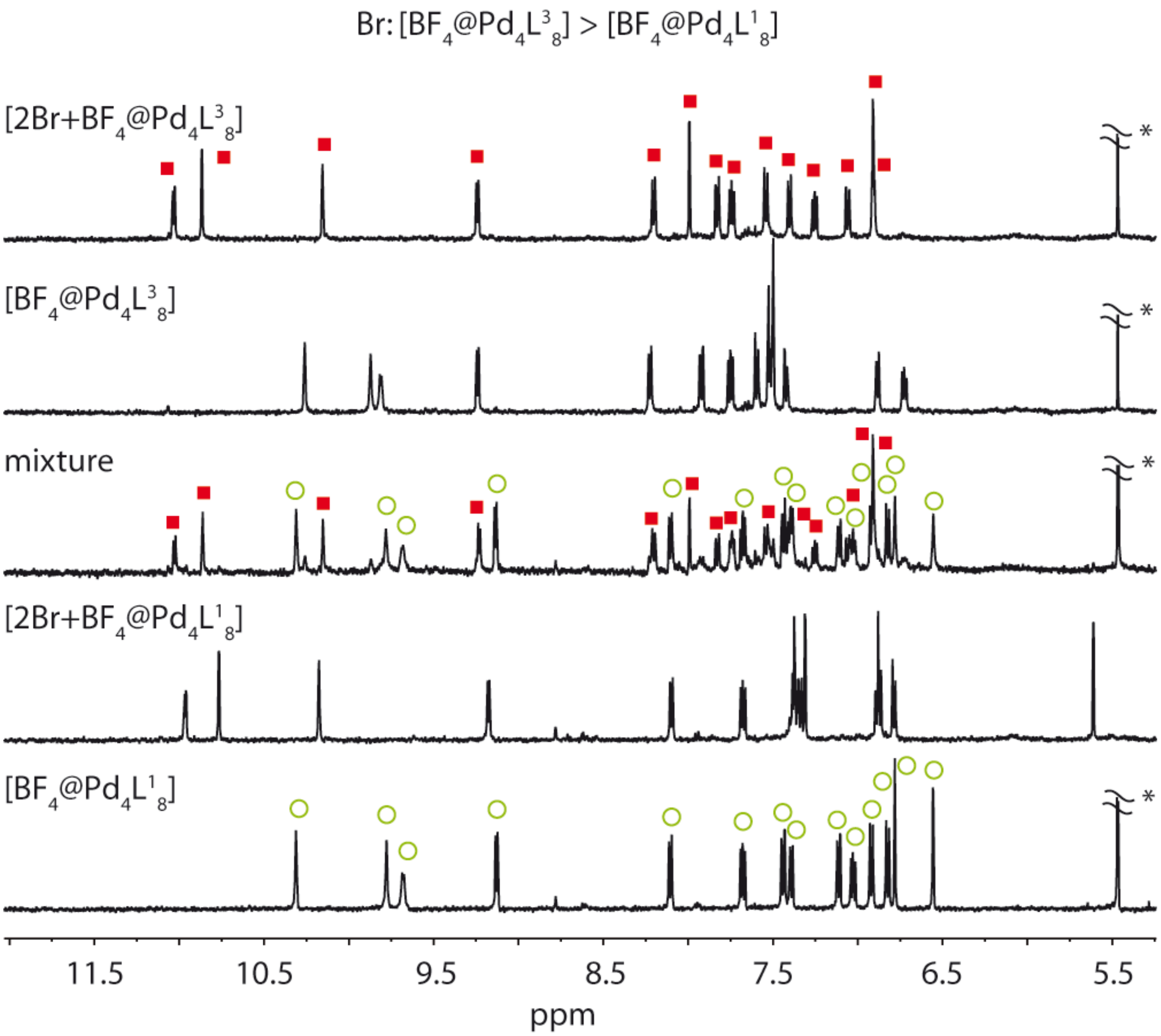

Figure SI-21: ^{1}H NMR titration (500 MHz, 298 K, CD$_3$CN): A competition experiment between [BF$_4$@Pd$_4$$\mathbf{L}^{\mathbf{1}}_8$](BF$_4$)$_7$ and [BF$_4$@Pd$_4$$\mathbf{L}^{\mathbf{3}}_8$](BF$_4$)$_7$ for the binding of the bromide anion shows that the latter one is the better binder. The [BF$_4$@Pd$_4$$\mathbf{L}^{\mathbf{1}}_8$](BF$_4$)$_7$, [2Br+BF$_4$@Pd$_4$$\mathbf{L}^{\mathbf{1}}_8$](BF$_4$)$_5$, [BF$_4$@Pd$_4$$\mathbf{L}^{\mathbf{3}}_8$](BF$_4$)$_7$ and [2Br+BF$_4$@Pd$_4$$\mathbf{L}^{\mathbf{3}}_8$](BF$_4$)$_5$ spectra are printed as reference. * = impurity.

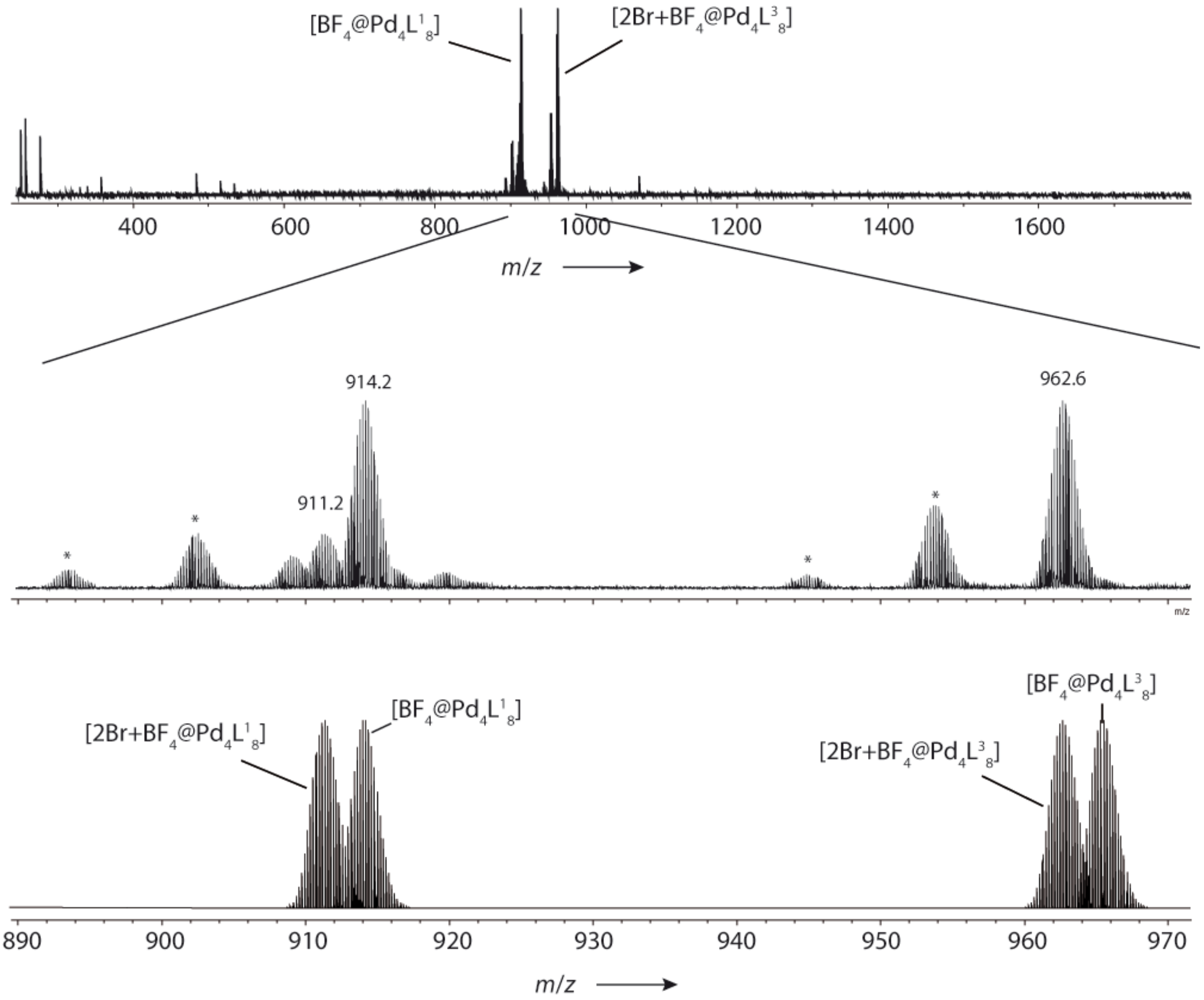

Figure SI-22: The ESI mass spectrum (FTICR, positive mode, eluent CH$_3$CN) of the host-guest-complexes in the competition experiment of [BF$_4$@Pd$_4$**L**$^{\mathbf{1}}_8$](BF$_4$)$_7$ and [BF$_4$@Pd$_4$**L**$^{\mathbf{3}}_8$](BF$_4$)$_7$ with NBu$_4$Br clearly shows the higher affinity of the latter cage for chloride binding. * = contamination with Cl$^-$.

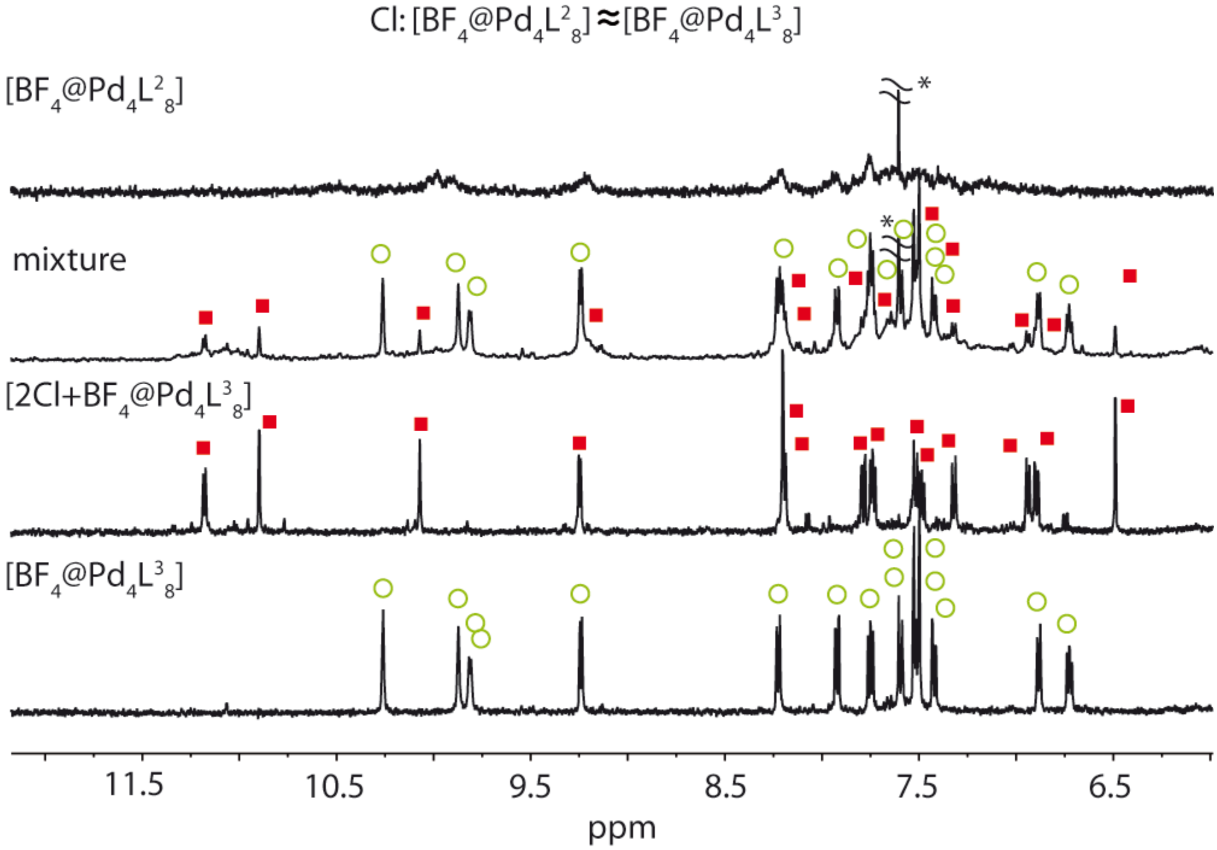

Figure SI-23: ^{1}H NMR titration (500 MHz, 298 K, CD_3CN): A competition experiment between $[BF_4@Pd_4\mathbf{L^2}_8](BF_4)_7$ and $[BF_4@Pd_4\mathbf{L^3}_8](BF_4)_7$ for the binding of the chloride anion shows that the double-cages show comparable affinities. The $[BF_4@Pd_4\mathbf{L^3}_8](BF_4)_7$, $[2Cl+BF_4@Pd_4\mathbf{L^3}_8](BF_4)_5$ and $[BF_4@Pd_4\mathbf{L^2}_8](BF_4)_7$ spectra are printed as reference.

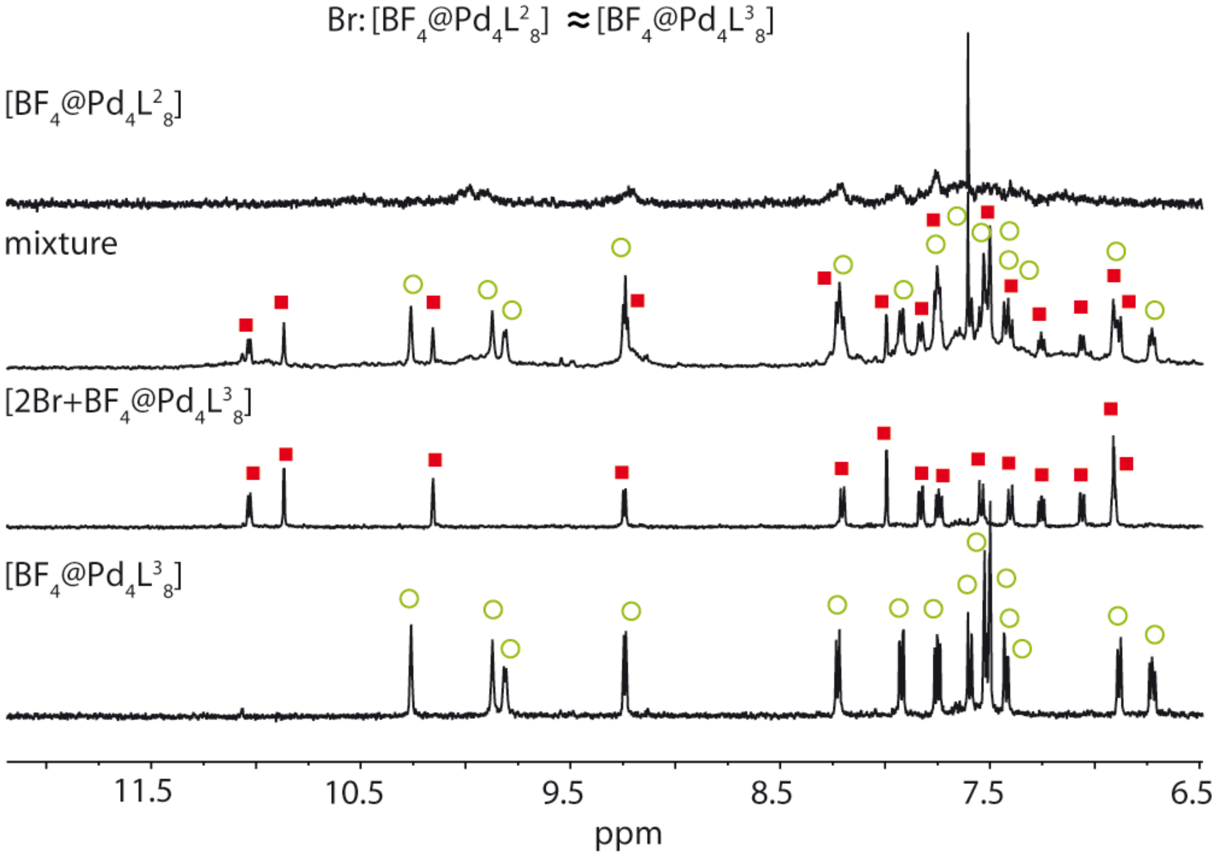

Figure SI-24: ^{1}H NMR titration (500 MHz, 298 K, CD$_3$CN): A competition experiment between [BF$_4$@Pd$_4$**L^2**$_8$](BF$_4$)$_7$ and [BF$_4$@Pd$_4$**L^3**$_8$](BF$_4$)$_7$ for the binding of the bromide anion shows that the double-cages show comparable affinities. The [BF$_4$@Pd$_4$**L^3**$_8$](BF$_4$)$_7$, [2Br+BF$_4$@Pd$_4$**L^3**$_8$](BF$_4$)$_5$ and [BF$_4$@Pd$_4$**L^2**$_8$](BF$_4$)$_7$ spectra are printed as reference.

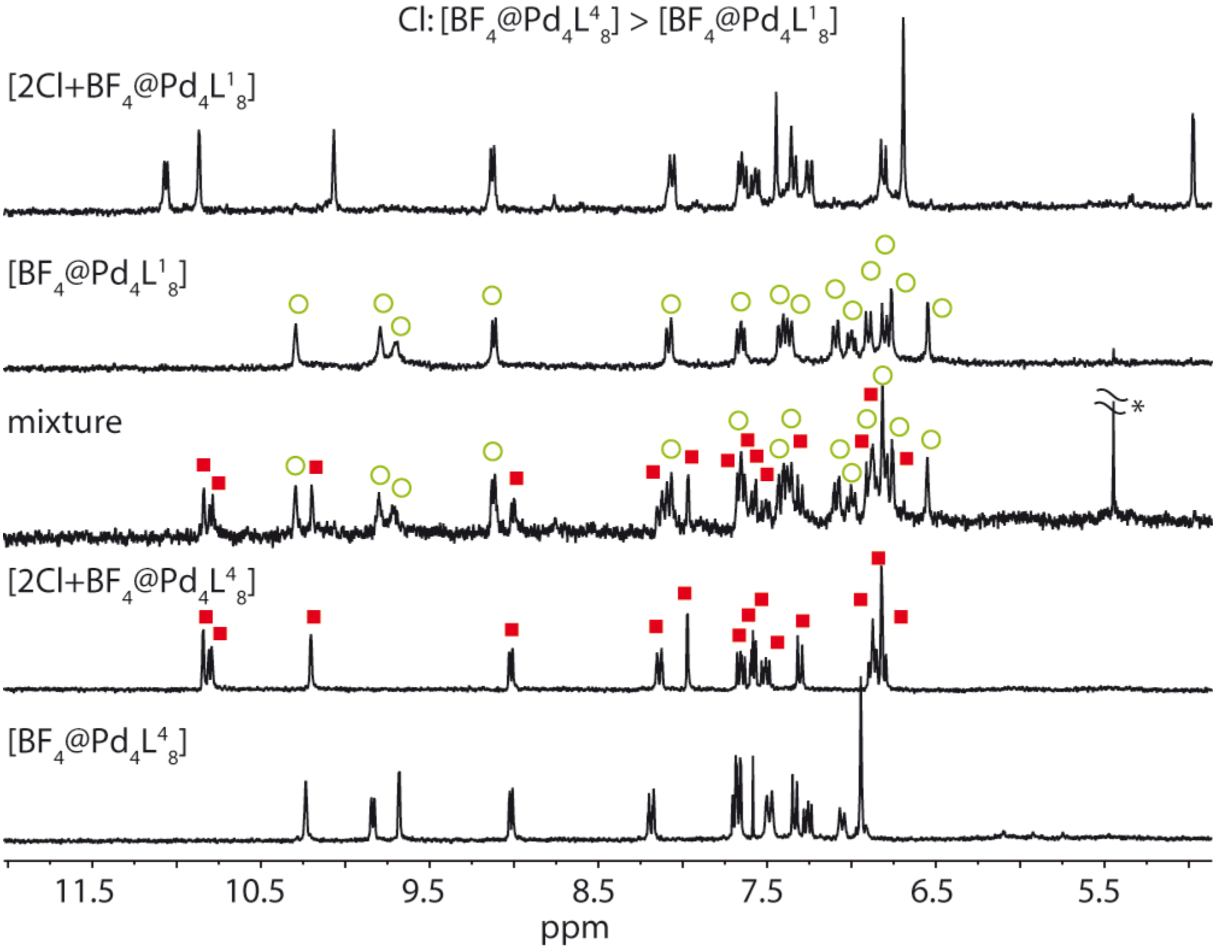

Figure SI-25: ^{1}H NMR titration (500 MHz, 298 K, CD_3CN): A competition experiment between $[BF_4@Pd_4\mathbf{L}^{\mathbf{1}}_8](BF_4)_7$ and $[BF_4@Pd_4\mathbf{L}^{\mathbf{4}}_8](BF_4)_7$ for the binding of the chloride anion shows that the latter one is the better binder. The $[BF_4@Pd_4\mathbf{L}^{\mathbf{1}}_8](BF_4)_7$, $[2Cl+BF_4@Pd_4\mathbf{L}^{\mathbf{1}}_8](BF_4)_5$, $[BF_4@Pd_4\mathbf{L}^{\mathbf{4}}_8](BF_4)_7$ and $[2Cl+BF_4@Pd_4\mathbf{L}^{\mathbf{4}}_8](BF_4)_5$ spectra are printed as reference. * = impurity.

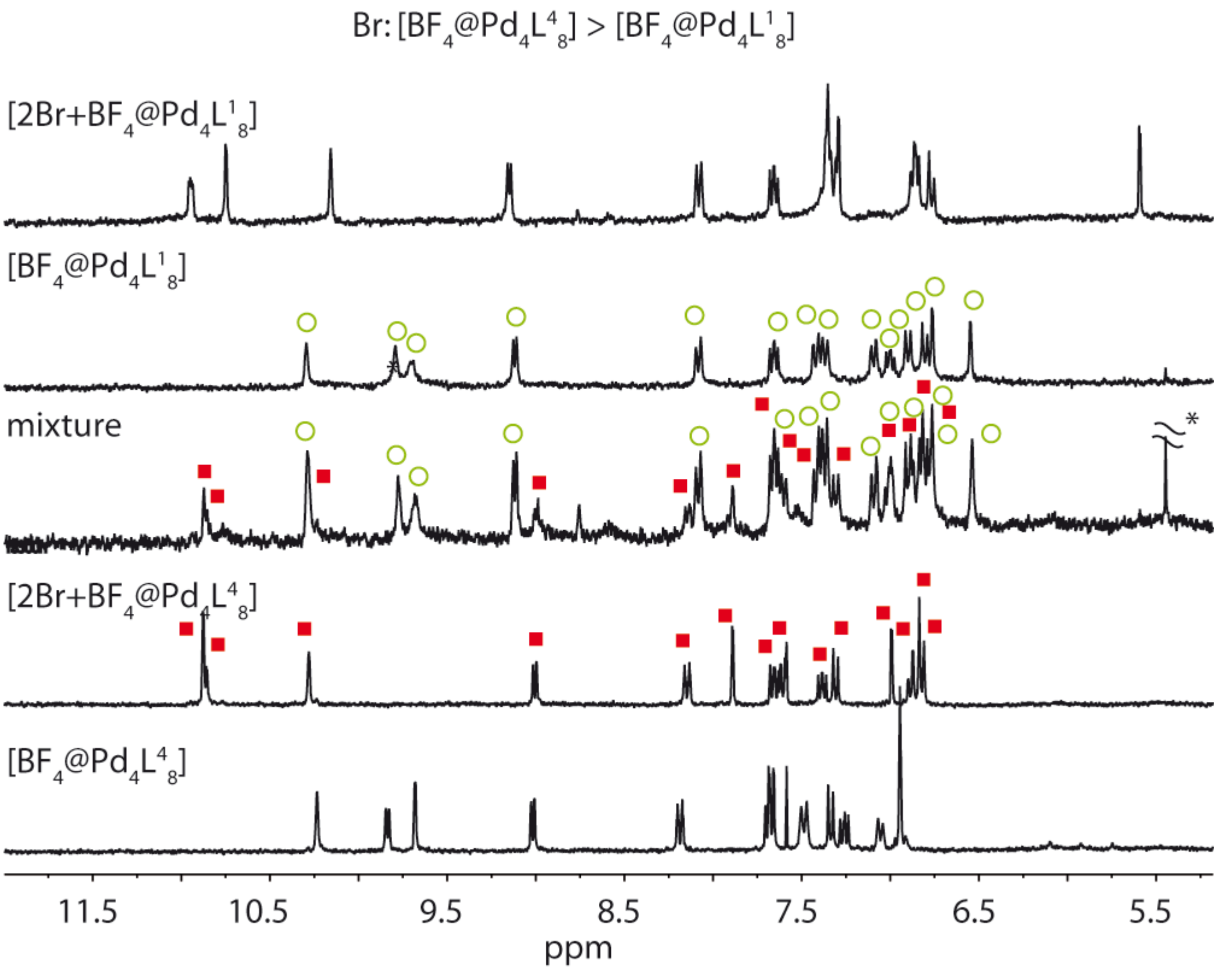

Figure SI-26: ^{1}H NMR titration (500 MHz, 298 K, CD_3CN): A competition experiment between $[BF_4@Pd_4\mathbf{L}^1_8](BF_4)_7$ and $[BF_4@Pd_4\mathbf{L}^4_8](BF_4)_7$ for the binding of the bromide anion shows that the latter one is the better binder. The $[BF_4@Pd_4\mathbf{L}^1_8](BF_4)_7$, $[2Br+BF_4@Pd_4\mathbf{L}^1_8](BF_4)_5$, $[BF_4@Pd_4\mathbf{L}^4_8](BF_4)_7$ and $[2Br+BF_4@Pd_4\mathbf{L}^4_8](BF_4)_5$ spectra are printed as reference. * = impurity.

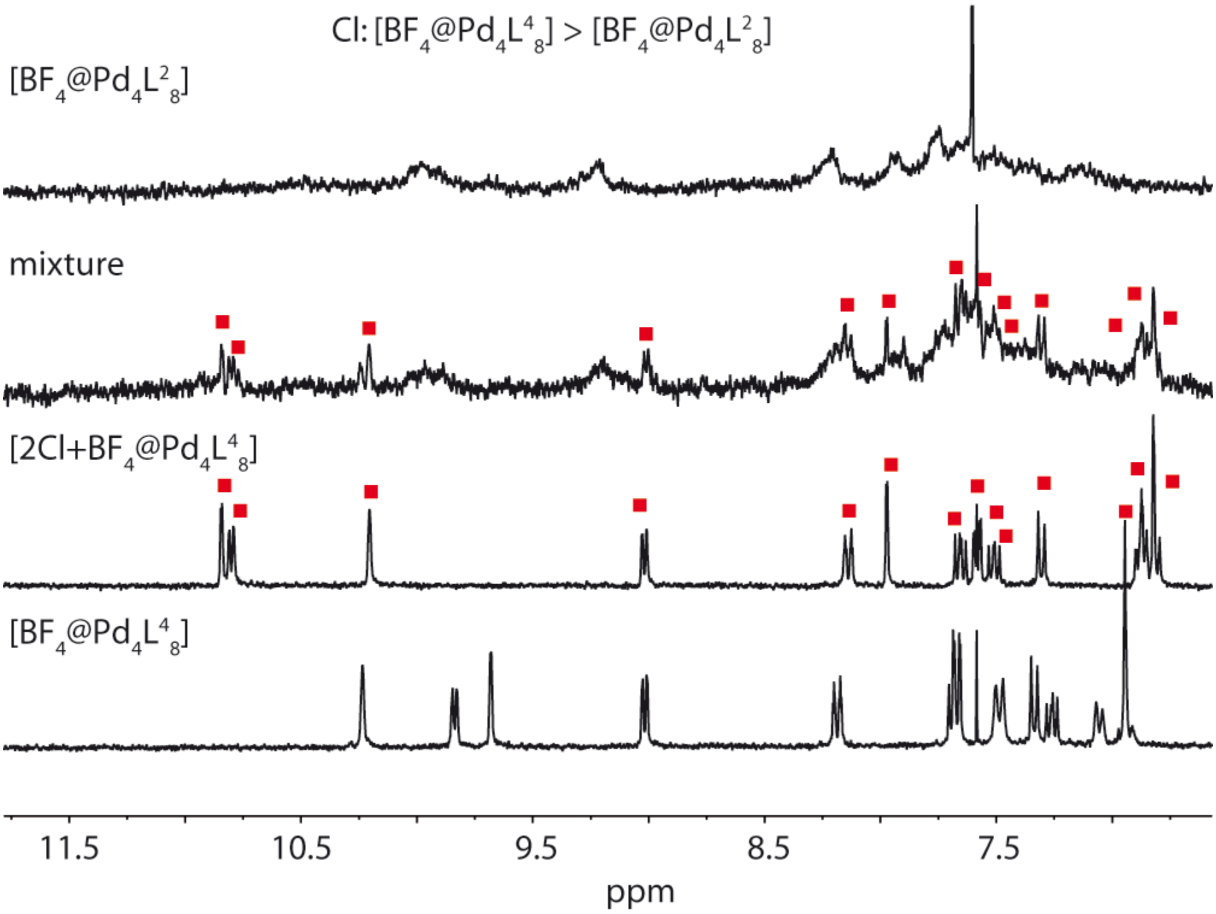

Figure SI-27: ^{1}H NMR titration (500 MHz, 298 K, CD$_3$CN): A competition experiment between [BF$_4$@Pd$_4$**L^2**$_8$](BF$_4$)$_7$ and [BF$_4$@Pd$_4$**L^4**$_8$](BF$_4$)$_7$ for the binding of the chloride anion shows that the latter one is the better binder. The [BF$_4$@Pd$_4$**L^2**$_8$](BF$_4$)$_7$, [2Cl+BF$_4$@Pd$_4$**L^4**$_8$](BF$_4$)$_5$ and [BF$_4$@Pd$_4$**L^4**$_8$](BF$_4$)$_7$ spectra are printed as reference.

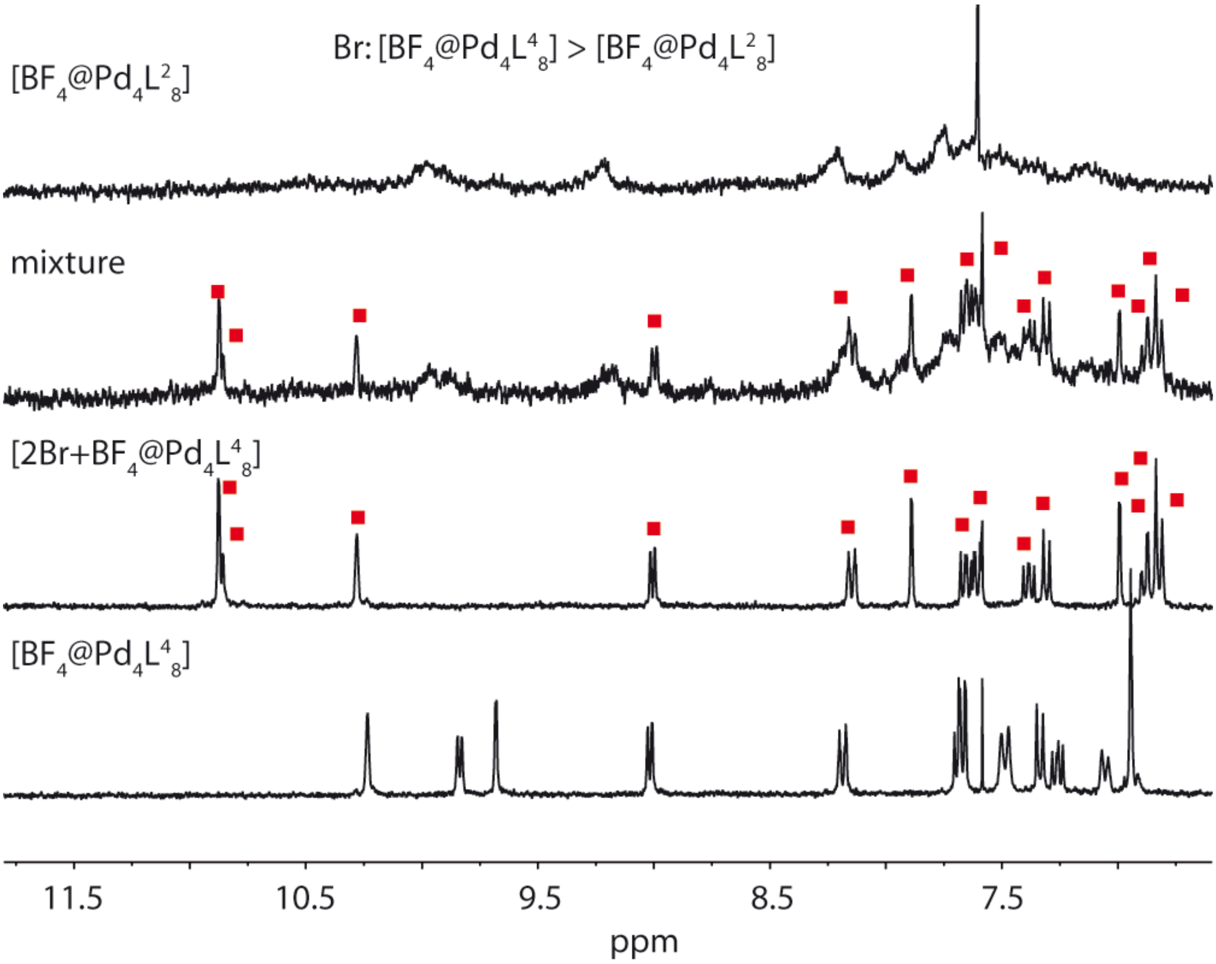

Figure SI-28: ^{1}H NMR titration (500 MHz, 298 K, CD_3CN): A competition experiment between $[BF_4@Pd_4\mathbf{L^2}_8](BF_4)_7$ and $[BF_4@Pd_4\mathbf{L^4}_8](BF_4)_7$ for the binding of the bromide anion shows that the latter one is the better binder. The $[BF_4@Pd_4\mathbf{L^2}_8](BF_4)_7$, $[2Br+BF_4@Pd_4\mathbf{L^4}_8](BF_4)_5$ and $[BF_4@Pd_4\mathbf{L^4}_8](BF_4)_7$ spectra are printed as reference.

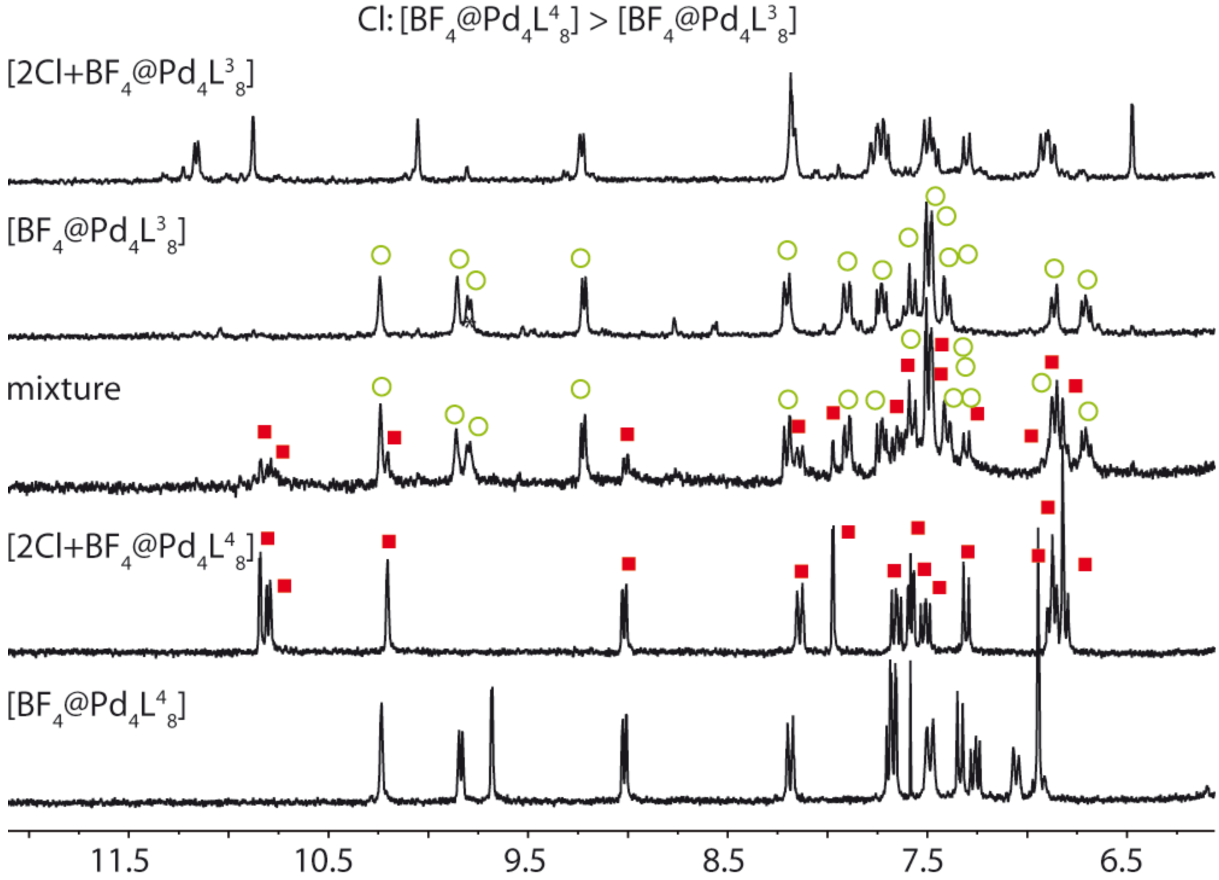

Figure SI-29: ^{1}H NMR titration (500 MHz, 298 K, CD_3CN): A competition experiment between $[BF_4@Pd_4\mathbf{L^3}_8](BF_4)_7$ and $[BF_4@Pd_4\mathbf{L^4}_8](BF_4)_7$ for the binding of the chloride anion shows that the latter one is the better binder. The $[BF_4@Pd_4\mathbf{L^3}_8](BF_4)_7$, $[2Cl+BF_4@Pd_4\mathbf{L^3}_8](BF_4)_5$, $[BF_4@Pd_4\mathbf{L^4}_8](BF_4)_7$ and $[2Cl+BF_4@Pd_4\mathbf{L^4}_8](BF_4)_5$ spectra are printed as reference. * = impurity.

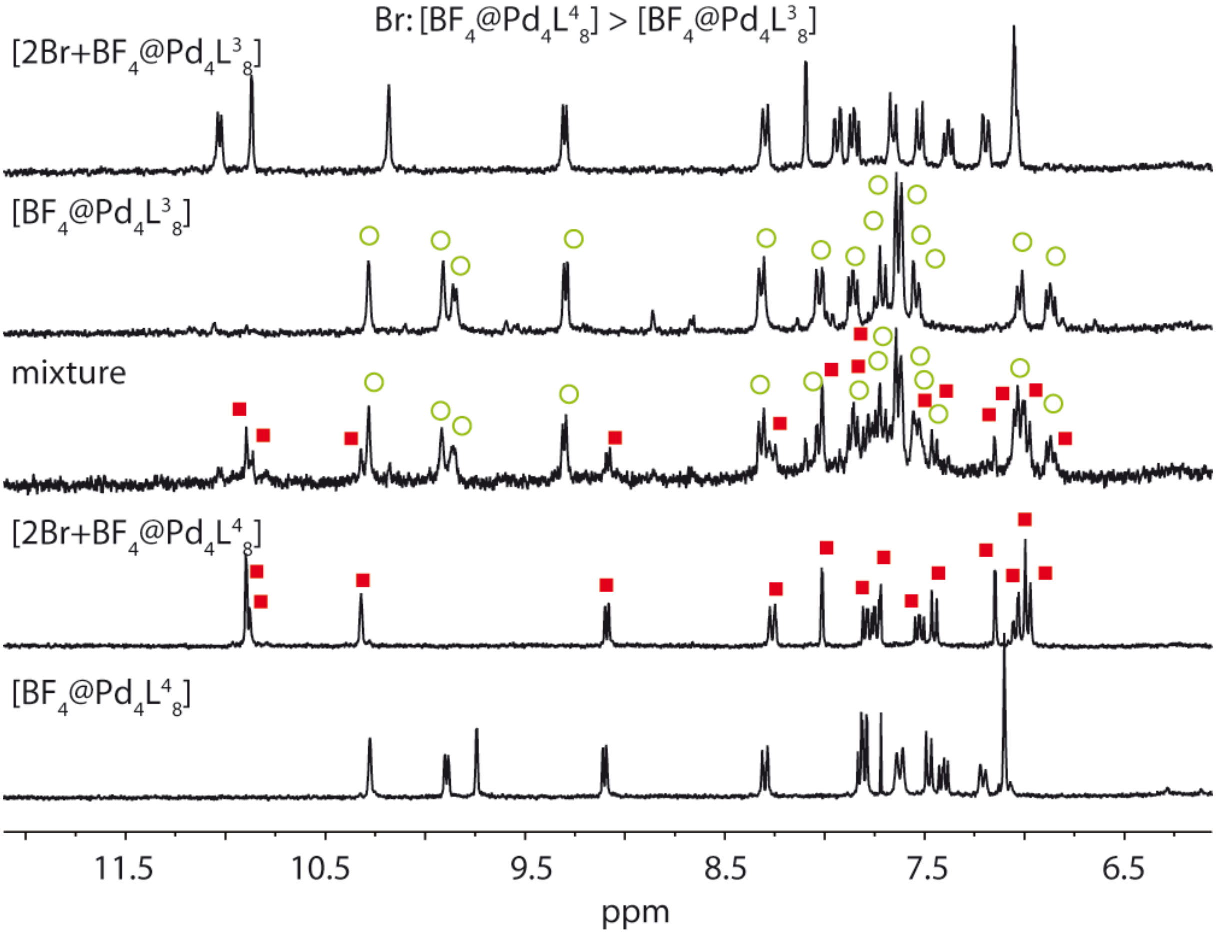

Figure SI-30: ^{1}H NMR titration (500 MHz, 298 K, CD$_3$CN): A competition experiment between [BF$_4$@Pd$_4$**L**$^{\mathbf{3}}_8$](BF$_4$)$_7$ and [BF$_4$@Pd$_4$**L**$^{\mathbf{4}}_8$](BF$_4$)$_7$ for the binding of the chloride anion shows that the latter one is the better binder. The [BF$_4$@Pd$_4$**L**$^{\mathbf{3}}_8$](BF$_4$)$_7$, [2Br+BF$_4$@Pd$_4$**L**$^{\mathbf{3}}_8$](BF$_4$)$_5$, [BF$_4$@Pd$_4$**L**$^{\mathbf{4}}_8$](BF$_4$)$_7$ and [2Br+BF$_4$@Pd$_4$**L**$^{\mathbf{4}}_8$](BF$_4$)$_5$ spectra are printed as reference. * = impurity.

4. ^{1}H,^{1}H-NOESY correlations

On the basis of the NOESY spectra of the coordination cages with different anions (X^- = Cl^-, Br^-) bound in the outer pockets, the NOESY signal intensities can be correlated with proton-proton distances. The data obtained from the crystal structure of $[BF_4@Pd_4\mathbf{L}^1_8](BF_4)_7$ was used to calculate the distances within the structures of $[2Cl+BF_4@Pd_4\mathbf{L}^1_8](BF_4)_5$ and $[2Br+BF_4@Pd_4\mathbf{L}^1_8](BF_4)_7$ according to our previously published method:[2]

The relative integral I_{rel} of an NOE signal depends on the interatomic distance d (a = proportionality factor).

$$I_{\mathrm{rel}} = a \cdot d^{-6}$$

To calculate the atomic distances, the interatomic distance d has to be written as a function of the measured integral.

$$d = a \cdot I_{\mathrm{rel}}{}^{-1/6}$$

To obtain reliable distances, the experimental conditions for the measurement of all NOESY spectra were held as constant as possible. Each individual proton-proton crosspeak in the NOESY spectrum of $[BF_4@Pd_4\mathbf{L}^1_8](BF_4)_7$ was compared to the corresponding crosspeak for $[2X+BF_4@Pd_4\mathbf{L}^1_8](BF_4)_5$ with X = Cl^-, Br^-. To minimize the error, one of the diagonal signal's integral was set to I = 1. The two cross-peak signal intensities I_1 and I_2 were averaged. The distances d_X in $[2X+BF_4@Pd_4\mathbf{L}^1_8](BF_4)_5$ were calculated according to the following equation:

$$d_{\mathrm{X}} = d_{\mathrm{BF_4}} \cdot \frac{I_{\mathrm{rel,X}}{}^{-1/6}}{I_{\mathrm{rel,BF_4}}{}^{-1/6}}$$

All signals used for the correlation show contribution of two protons to the observed integral I_{rel}, so the NOE signal integrals could not be directly compared to the distances in the crystal structure. Artificial distances d' were calculated from the two contributing distances d_1 and d_2 using the following equation.

$$d' = (d_1^{-6} + d_2^{-6})^{-1/6}$$

An analogous distance d'^* was extracted from a series of molecular models and compared to the artificial distances d'.

Errors for the distances Δd_X were calculated using the integral-dependent maximum error. The integral error ΔI_{rel} was obtained from the standard deviation of the two averaged integral values and the contribution of the noise as an absolute part $\Delta I_{rel,\ noise}$ = 0.0004 obtained from the noise level of the NOESY spectra.

$$\Delta d_{\mathrm{X}} = \left|\frac{\partial d_{\mathrm{X}}}{\partial I_{\mathrm{rel,BF_4}}} \cdot \Delta I_{\mathrm{rel,BF_4}}\right| + \left|\frac{\partial d_{\mathrm{X}}}{\partial I_{\mathrm{rel,X}}} \cdot \Delta I_{\mathrm{rel,X}}\right|$$

$$\Delta d_{\mathrm{X}} = \left|-\frac{1}{6} \cdot d_{\mathrm{BF_4}} \cdot \frac{I_{\mathrm{rel,X}}{}^{-7/6}}{I_{\mathrm{rel,BF_4}}{}^{-1/6}} \cdot \Delta I_{\mathrm{rel,BF_4}}\right| + \left|\frac{1}{6} \cdot d_{\mathrm{BF_4}} \cdot \frac{I_{\mathrm{rel,X}}{}^{-1/6}}{I_{\mathrm{rel,BF_4}}{}^{5/6}} \cdot \Delta I_{\mathrm{rel,X}}\right|$$

A series of models for [2X+BF_4@Pd_4**L**$^1_8$](BF_4)$_5$ was generated by applying different values of the translation Δ*d* on the crystal structure of [BF_4@Pd_4**L**$^1_8$](BF_4)$_7$. In order to identify a suitable model representing the real solution structure of [2X+BF_4@Pd_4**L**$^1_8$](BF_4)$_5$, the deviations of these distances from those obtained from the NOESY correlation were quantified by calculation of the *Q*-factor for each model.

$$Q = \left\{ \frac{\sum_{i=1}^{N} \left(d_{\mathrm{i}}^{\mathrm{exp}} - d_{\mathrm{i}}^{\mathrm{calc}} \right)^2}{\sum_{i=1}^{N} \left(d_{\mathrm{i}}^{\mathrm{exp}} \right)^2} \right\}^{1/2}$$

A perfect agreement of the model and the experiment would result in *Q* = 0.

Table 1: NOE signal intensities and proton proton distances for [BF_4@Pd_4**L**$^1_8$](BF_4)$_7$ and [2C+IBF_4@Pd_4**L**$^1_8$](BF_4)$_5$

[3BF_4@Pd_4**L**$^1_8$]									
	NOE						Crystal Structure		
Protons	I_1	I_2	I	ΔI			d_1 [Å]	d_2 [Å]	d' [Å]
g -> f'	0,0155	0,0108	0,0132	0,0033			4,948	5,340	5,405
g -> e'	0,0027	0,0025	0,0026	0,0001			5,817	6,419	4,559
f' -> a	0,0377	0,0324	0,0351	0,0037			3,017	3,320	2,800
e' -> a	0,0239	0,0269	0,0254	0,0021			3,377	3,716	3,135
[2Cl+BF4@Pd_4**L**$^1_8$]									
	NOE				Correlation		Model distances (best fit)	Model distances (best fit)	Model distances (best fit)
Protons	I_1	I_2	I	ΔI	d' [Å]	Δd' [Å]	d_1* [Å]	d_1* [Å]	d_1* [Å]
g -> f'	0,0339	0,0298	0,0319	0,0029	4,664	0,252	4,220	4,674	3,926
g -> e'	0,0064	0,0058	0,0061	0,0004	3,955	0,123	5,860	5,194	4,863
f' -> a	0,0187	0,0248	0,0218	0,0043	3,032	0,149	2,934	3,245	2,728
e' -> a	0,0173	0,0128	0,0151	0,0032	3,420	0,152	3,274	3,623	3,045
[2Br+BF4@Pd_4**L**$^1_8$]									
	NOE				Correlation		Model distances (best fit)	Model distances (best fit)	Model distances (best fit)
Protons	I_1	I_2	I	ΔI	d' [Å]	Δd' [Å]	d_1* [Å]	d_1* [Å]	d_1* [Å]
g -> f'	0,0148	0,0147	0,0148	0,0001	5,303	0,204	4,801	5,205	4,432
g -> e'	0,0045	0,0044	0,0045	0,0001	4,169	0,041	5,690	6,304	5,295
f' -> a	0,0271	0,0223	0,0247	0,0034	2,968	0,123	2,985	3,291	2,773
e' -> a	0,0202	0,0176	0,0189	0,0018	3,293	0,101	3,686	3,343	3,105

Table 1 shows that the best model for [2Cl+BF_4@Pd_4**L**$^1_8$](BF_4)$_5$ is found at an inner Pd-Pd distance of *d*(Pd-Pd) = 9.65 Å. This is a change of 0.80 Å compared to [BF_4@Pd_4**L**$^1_8$](BF_4)$_7$, where *d*(Pd-Pd) is 8.85 Å.

The best model for [2Br+BF_4@Pd_4**L**$^1_8$](BF_4)$_5$ is found at an inner Pd-Pd distance of *d*(Pd-Pd) = 9.05 Å. This is a change of 0.20 Å compared to [BF_4@Pd_4**L**$^1_8$](BF_4)$_7$, where *d*(Pd-Pd) is 8.85 Å.

5. Calculations of the NMR shifts after binding of halide anions

General procedure

Relative NMR chemical shifts $\Delta\delta$ of the protons H_a and $H_{a'}$ were calculated using the GIAO method as implemented in Gaussian '09.[3] A fragment of the double cage structure containing one inner Pd(II) ion and two BF_4^- anions was used for the calculations (s. Fig. SI-31). In order to reduce computational costs, the hexyl substituents were truncated to leave methyl groups. The DFT computation was performed on the B3LYP/LANL2DZ level of theory using the default solvation model (IEFPCM) with the solvent acetonitrile. The rather small basis set was used as a compromise between computational costs and the large system size including a transition metal cation. For comparison, a smaller fragment (only one ligand backbone, two neighboring pyridines, one BF_4^- anion, but without the palladium(II) cation) was calculated with a larger basis set (6-311G-(d,p)) and resulted in similar trends for the $\Delta\delta$ values (not shown).

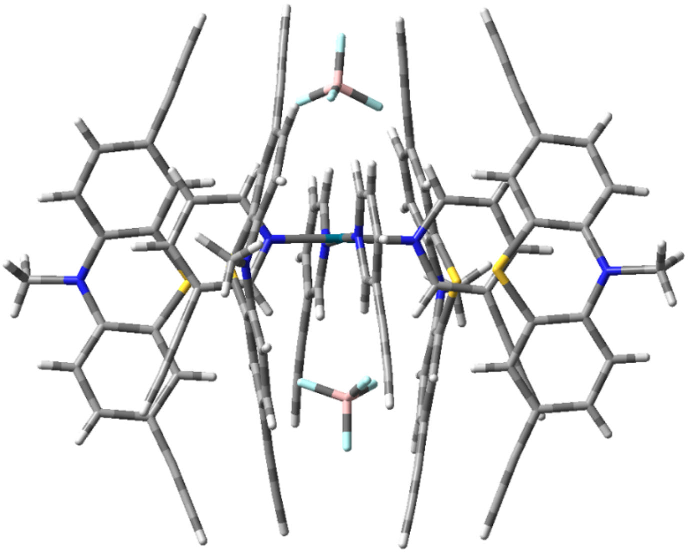

Figure SI-31: Fragment used for the computation of relative NMR chemical shifts by Gaussian '09.

The results of the relative NMR chemical shift computations of the protons H_a and $H_{a'}$ for all four coordination cages $[BF_4@Pd_4\mathbf{L}^{\mathbf{n}}_8](BF_4)_7$ with n = 1-4 and the experimental values (s. also Tab. 1) are shown in Fig. SI-32. The $\Delta\delta$ value is the difference between the shifts of the H_a and $H_{a'}$ protons of $[BF_4@Pd_4\mathbf{L}^{\mathbf{n}}_8](BF_4)_7$ and $[2X+BF_4@Pd_4\mathbf{L}^{\mathbf{n}}_8](BF_4)_5$ with X = Cl^-, Br^-.

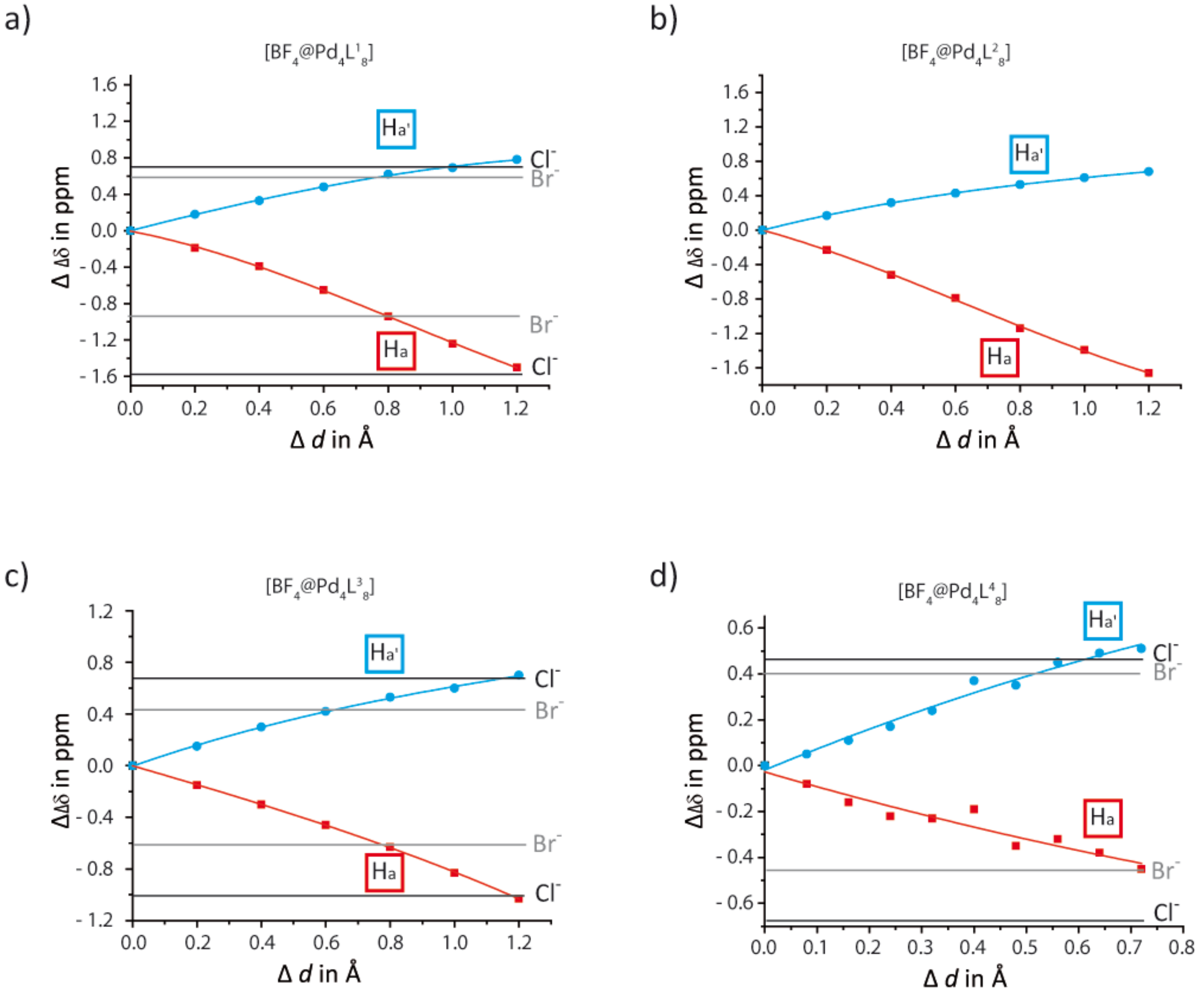

Figure SI-32: Results of the computation of relative NMR chemical shifts for a) $[BF_4@Pd_4\mathbf{L}^1_8]$, b) $[BF_4@Pd_4\mathbf{L}^2_8]$, c) $[BF_4@Pd_4\mathbf{L}^3_8]$ and d) $[BF_4@Pd_4\mathbf{L}^4_8]$. The horizontal lines assign the experimental differences between the shifts of the cages $[BF_4@Pd_4\mathbf{L}^n_8]$ with n = 1, 3, 4 and the cages $[2X{+}BF_4@Pd_4\mathbf{L}^n_8]$ with X = Cl^-, Br^-. No experimental values could be obtained for $[BF_4@Pd_4\mathbf{L}^2_8]$ since the compound shows very broad signals in the ^{1}H NMR.

Table SI-2: Summary of the differences in chemical shifts of the protons H_a and $H_{a'}$ upon anion binding.

		Δshift H_a in ppm	Δshift $H_{a'}$ in ppm
Cl	$[BF_4@Pd_4L^1_8]$	- 1.57	0.70
	$[BF_4@Pd_4L^2_8]$	x	x
	$[BF_4@Pd_4L^3_8]$	- 1.01	0.68
	$[BF_4@Pd_4L^4_8]$	- 0.70	0.44
Br	$[BF_4@Pd_4L^1_8]$	- 0.94	0.59
	$[BF_4@Pd_4L^2_8]$	x	x
	$[BF_4@Pd_4L^3_8]$	-0.62	0.44
	$[BF_4@Pd_4L^4_8]$	-0.49	0.38

Table SI-3: Summary of the Pd-Pd distances in the coordination cages. In cases of [BF$_4$@Pd$_4$**L**$^{\mathbf{1}}_8$], [BF$_4$@Pd$_4$**L**$^{\mathbf{2}}_8$] and [BF$_4$@Pd$_4$**L**$^{\mathbf{4}}_8$] the distances are obtained from the X-ray structure.[1a,1b] The values for [BF$_4$@Pd$_4$**L**$^{\mathbf{3}}_8$] are taken from the DFT-calculated structure.[1b]

	d(Pd-Pd)$_{\text{monocage}}$ in Å	d (Pd$_{\text{outer}}$-Pd$_{\text{inner}}$) in Å	d (Pd$_{\text{inner}}$-Pd$_{\text{inner}}$) in Å
[BF$_4$@Pd$_4$L$^1_8$]	17.62	8.77	8.85
[BF$_4$@Pd$_4$L$^2_8$]	16.77	8.16	8.63
[BF$_4$@Pd$_4$L$^3_8$]	16.55	8.42-8.52	8.03
[BF$_4$@Pd$_4$L$^4_8$]	16.34	8.09	8.25

6. Model calculations for the double-cage systems

In order to calculate optimal Δ*d* and *R* (denoted as *d*(N,N) = *d*(Pd,Pd) in the main text) values for the cage systems interacting with halide anions in the outer pockets, we applied the push-and-pull model adopted in our previous study of $\mathbf{L^4}$.[4] The fitting range for the anion Cl^- was expanded up to 10.5 Å, BF_4^- to 9.8 Å, and the same distance range as in Cl^- was adopted for Br^-. The scheme in Fig. SI-33 shows our simplified model for the host-guest interactions. The only variable for *a* fixed *R* is the distance r_2 in the inner pocket. The interaction energies are computed by splitting the total potential into three separate terms, each being calculated at the DF-MP2/cc-pVTZ level of theory (cc-pVTZ-PP for Pd, in combination with the ECP28MDF pseudopotential).[5,6] Each subsystem consists of two Pd(II) complexes with four pyridines, with the anion being placed in the middle of the two planes. The distance *r* between the two planes is varied and the interaction energy calculated. In the case of BF_4^-, since the anion is not perfectly spherical, the structure was optimized, keeping the planes fixed. The optimisations were carried out at the BP86/def2-SVP level of theory with the ORCA program package.[7] The wave function calculations were carried out with Molpro2010.1.[8]

The potential profiles were calculated for each of the three different anions and were then fitted to a linear combination of gaussian functions through the use of the OGOLEM program.[9,10] In the case of the halides, 7 Gaussian functions were used. For BF_4^- only 4 Gaussians were applied to avoid overfitting of the profile. The results are shown in Figs. SI-34.

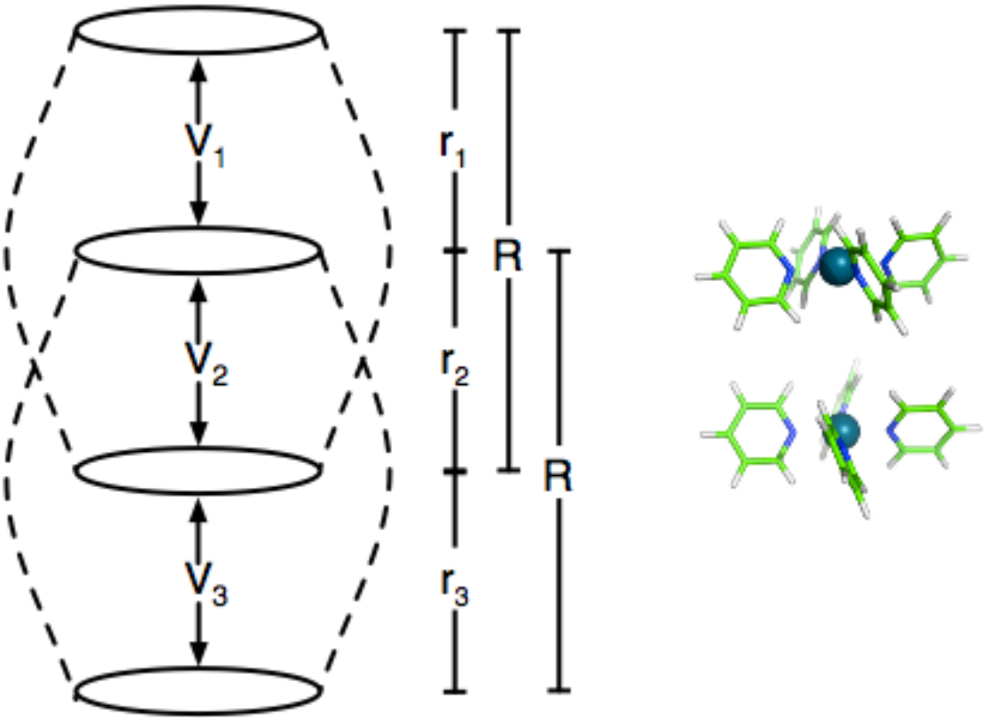

Fig. SI-33: Push-and-pull model for anion binding. The three pockets are represented by three different subsystems. The total potential is given by $V=V_1+V_2+V_3$, which upon fixing the distance *R*, is dependent on a single variable (in our case, the distance r_2).

Table SI-4: Calculated Pd_{inner}-Pd_{inner} distances used for Fig. 5.

	$\mathbf{L^1}$	$\mathbf{L^2}$	$\mathbf{L^3}$	$\mathbf{L^4}$
$BF4^-$	9.17±0.17	8.39±0.14	8.20±0.20	8.09±0.25
Br^-	9.80±0.09	9.46±0.32	9.28±0.33	9.01±0.41
Cl^-	9.80±0.06	9.78±0.18	9.63±0.26	9.07±0.33

The theoretical error bars are based on a 1 kcal/mol tolerance for each given minimum. The estimated errors for the distance are computed as the average deviation of the upper and lower values. The distances for BF_4^- and Cl^- in $\mathbf{L^4}$ are the same as featured in a previous work. The error bar for the Cl^- distance has been reviewed based on a new parameterization of the BF_4^- inner pocket potential.

a) BF_4

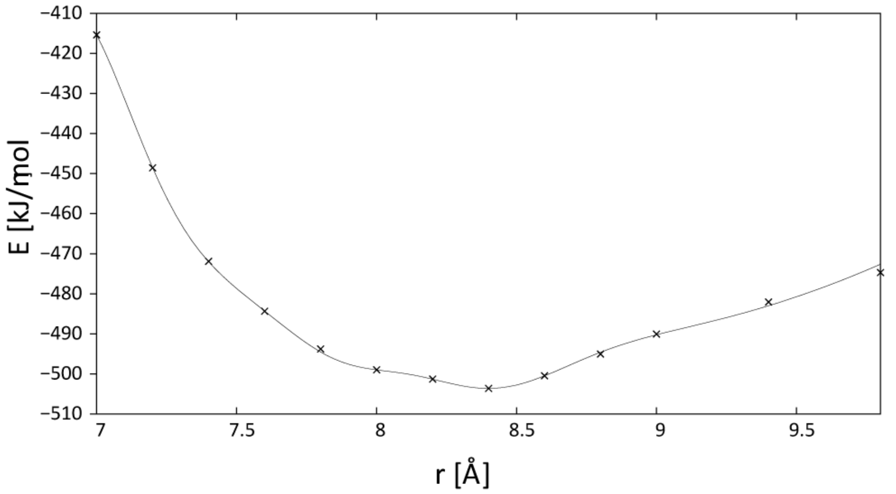

b) Br

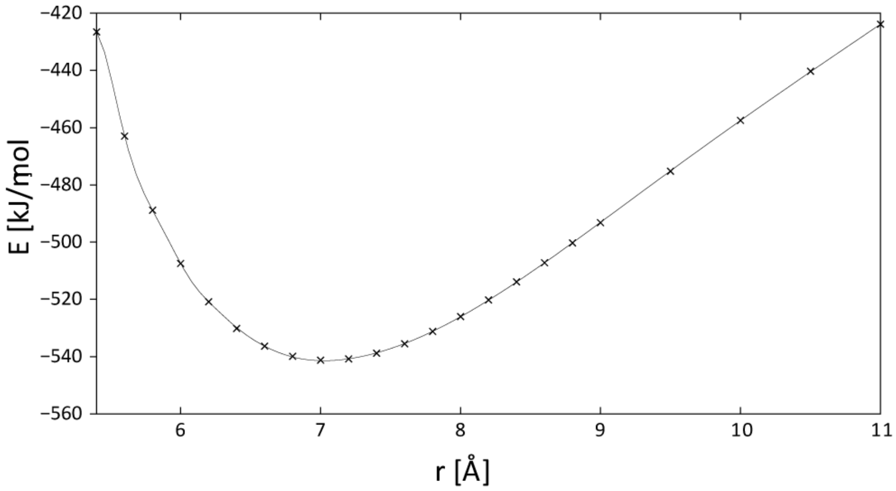

c) Cl

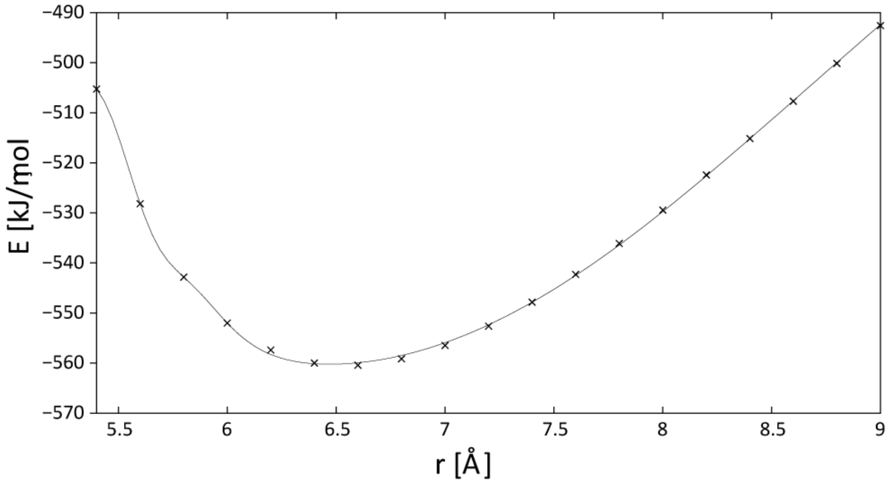

Fig. SI-34: a) DF-MP2 interaction energy profile (in kJ/mol) for BF_4^- interacting with two Pd(II)(pyridine)$_4$ planes. b) DF-MP2 interaction energy profile (in kJ/mol) for Br^- interacting with two Pd(II) planes. c) DF-MP2 interaction energy profile (in kJ/mol) for Cl^- interacting with two Pd(II) planes.

References

[1] (a) S. Freye, J. Hey, A. Torras-Galán, D. Stalke, R. Herbst-Irmer, M. John, G. H. Clever, *Angew. Chem. Int. Ed.*, 2012, **51**, 2191; (b) M. Frank, J. Hey, I. Balcioglu, Y.-S. Chen, D. Stalke, T. Suenobu, S. Fukuzumi, H. Frauendorf, G. H. Clever, *Angew. Chem. Int. Ed.*, 2013, DOI: anie.201302536.

[2] S. Freye, D. M. Engelhard, M. John, G. H. Clever, *Chem. Eur. J.*, 2013, **19**, 2114.

[3] Gaussian 09, M. J. Frisch, G. W. Trucks, H. B. Schlegel, G. E. Scuseria, M. A. Robb, J. R. Cheeseman, G. Scalmani, V. Barone, B. Mennucci, G. A. Petersson, H. Nakatsuji, M. Caricato, X. Li, H. P. Hratchian, A. F. Izmaylov, J. Bloino, G. Zheng, J. L. Sonnenberg, M. Hada, M. Ehara, K. Toyota, R. Fukuda, J. Hasegawa, M. Ishida, T. Nakajima, Y. Honda, O. Kitao, H. Nakai, T. Vreven, J. A. Montgomery, Jr., J. E. Peralta, F. Ogliaro, M. Bearpark, J. J. Heyd, E. Brothers, K. N. Kudin, V. N. Staroverov, R. Kobayashi, J. Normand, K. Raghavachari, A. Rendell, J. C. Burant, S. S. Iyengar, J. Tomasi, M. Cossi, N. Rega, J. M. Millam, M. Klene, J. E. Knox, J. B. Cross, V. Bakken, C. Adamo, J. Jaramillo, R. Gomperts, R. E. Stratmann, O. Yazyev, A. J. Austin, R. Cammi, C. Pomelli, J. W. Ochterski, R. L. Martin, K. Morokuma, V. G. Zakrzewski, G. A. Voth, P. Salvador, J. J. Dannenberg, S. Dapprich, A. D. Daniels, O. Farkas, J. B. Foresman, J. V. Ortiz, J. Cioslowski and D. J. Fox, Gaussian, Inc., Wallingford CT, **2009**.

[4] J. M. Dieterich, G. H. Clever and R. A. Mata, Phys. Chem. Chem. Phys., 2012, 14, 12746-12749.

[5] T. H. Dunning, J. Chem. Phys., 1989, 90, 1007.

[6] K. Peterson, D. Figgen, M. Dolg and H. Stoll, J. Chem. Phys., 2007, 126, 124101.

[7] F. Neese, Orca: An Ab Initio, DFT and Semiempirical electronic structure package v2.8, 2011.

[8] H.-J. Werner, P. J. Knowles, G. Knizia, F. R. Manby and M. Schütz, et al., MOLPRO, version 2010.1, a package of ab initio programs, 2010, see http://www.molpro.net.

[9] J. M. Dieterich and B. Hartke, Mol. Phys., 2010, 108, 279.

[10] J. M. Dieterich and B. Hartke, J. Comput. Chem., 2011, 32, 1377.